AMPK deficiency blocks the hypoxic ventilatory response and thus precipitates hypoventilation and apnea

Mahmoud, Amira D; Lewis, Sophronia; Jurii, Lara; Udoh, Utibe-Abasi; Hartmann, Sandy; Jansen, Maurits A; Ogunbayo, Oluseye; Puggioni, Paolo; Holmes, Andrew; Kumar, Prem; Navarro-Dorado, Jorge; Foretz, Marc; Viollet, Benoit; Dutia, Mayank B; Marshall, Ian; Evans, A Mark

DOI:
10.1164/rccm.201508-1667OC

AJRCCM Articles in Press. Published on 15-December-2015 as 10.1164/rccm.201508-1667OC

AMPK deficiency blocks the hypoxic ventilatory response and thus precipitates hypoventilation and apnea

Amira D. Mahmoud[1], Sophronia Lewis[1], Lara Juričić[2], Utibe-Abasi Udoh[1], Sandy Hartmann[1], Maurits A. Jansen[2], Oluseye A. Ogunbayo[1], Paolo Puggioni[1], Andrew P. Holmes[3], Prem Kumar[3], Jorge Navarro-Dorado[1], Marc Foretz[4,5,6], Benoit Viollet[4,5,6], Mayank B. Dutia[1], Ian Marshall[7], A. Mark Evans[1]

[1]Centre for Integrative Physiology, [2]Centre for Cardiovascular Science and [7]Centre for Clinical Brain Sciences, College of Medicine and Veterinary Medicine, University of Edinburgh, Edinburgh, UK. [3]Institute of Clinical Sciences, University of Birmingham, Birmingham, UK. [4]Institut Cochin, INSERM U1016, [5]CNRS UMR and [6]Université Paris Descartes, Paris, France.

[*]**CORRESPONDING AUTHOR**: A. Mark Evans, Centre for Integrative Physiology, College of Medicine and Veterinary Medicine, Hugh Robson Building, University of Edinburgh, Edinburgh, EH8 9XD, UK. E-mail: mark.evans@ed.ac.uk

AUTHOR CONTRIBUTIONS: A.M.E. and A.D.M. wrote the manuscript. A.M.E., O.A.O., A.D.M. and S.H. developed the conditional *AMPK* knockout mice and performed genotyping. M.F. and B.V. developed the AMPK floxed mice. A.D.M. designed and validated primers. A.D.M., O.A.O., S.L. and A.M.E. performed RT-PCR. A.D.M., S.M. and A.M.E. performed plethysmography. A.D.M., S.M. A.M.E. and M.B.D. analyzed respiratory data. A.M.E., L.J., I.M., M.J., S.L. and A.D.M. performed magnetic resonance imaging and analysis. A.P.H. and P.K. performed afferent discharge blind and under subcontract at the University of Birmingham. U-A.U., J.N-D., M.D. and A.M.E. performed immunocytochemistry. A.D.M., S.L. and A.M.E. performed blood gas analyses. All authors discussed the results and provided feedback.

FUNDING: This work was primarily funded by the Wellcome Trust (WT081195MA), and was also supported by the British Heart Foundation (RG/12/14/29885).

RUNNING HEAD: AMPK protects against hypoventilation and apnea
DESCRIPTOR NUMBER: 8.8
WORD COUNT FOR BODY OF TEXT: 4182

AT A GLANCE COMMENTARY

Scientific Knowledge on the Subject: Ventilatory adjustments are critical to the body's capacity to accommodate deficits in oxygen availability during sleep and ascent to altitude. During hypoxia increased afferent discharge from the carotid bodies to the brainstem delivers increased ventilatory drive, which restores oxygen supply and protects against apnea. The precise molecular mechanisms involved remain unclear. However, natural selection in high-altitude populations has acted on the gene for the α1 catalytic subunit of the AMP-activated protein kinase (AMPK), which governs cell-autonomous adaptations during metabolic stress.

What This Study Adds to the Field: We demonstrate for the first time that AMPK deficiency leads to respiratory depression during hypoxia, characterized by hypoventilation and apnea rather than hyperventilation. Moreover, consequent deficits in the drive to breathe during hypoxia arise at the level of the brainstem, even where carotid body afferent input is normal. This identifies AMPK as a potential new target for therapeutic interventions for sleep disordered breathing associated with metabolic syndrome-related disorders and ascent to altitude.

This article has an online data supplement, which is accessible from this issue's table of content online at www.atsjournals.org

Abstract

Rationale: Modulation of breathing by hypoxia accommodates variations in oxygen demand and supply during, for example, sleep and ascent to altitude, yet the precise molecular mechanisms remain controversial. Among those genes influenced by natural selection in high-altitude populations is that for the AMP-activated protein kinase (AMPK) α1 catalytic subunit, which governs cell autonomous adaptations during metabolic stress.

Objective: We investigated whether or not AMPK-α1 and/or AMPK-α2 are required for the hypoxic ventilatory response and the mechanism of ventilatory dysfunctions arising from AMPK deficiency.

Methods: Experiments utilized plethysmography, electrophysiology, functional magnetic resonance imaging and immediate early gene (*cfos*) expression to assess the hypoxic ventilatory response of mice with conditional deletion of the *AMPK-α1* and/or *AMPK-α2* genes in catecholaminergic cells, which comprise the hypoxia-responsive respiratory network from carotid body to brainstem.

Measurements and Main Results: *AMPK-α1+α2* deletion virtually abolished the hypoxic ventilatory response, and ventilatory depression during hypoxia was exacerbated under anesthesia. Rather than hyperventilating, mice lacking *AMPK-α1+α2* exhibited hypoventilation and apnea during hypoxia, the primary precipitant being loss of *AMPK-α1* expression. However, the carotid bodies of *AMPK* knockouts remained exquisitely sensitive to hypoxia, contrary to the view that the hypoxic ventilatory response is solely determined by increased carotid body afferent input to the brainstem. Regardless, functional magnetic resonance imaging and *cfos* expression revealed reduced activation by hypoxia of well-defined dorsal and ventral brainstem nuclei.

Conclusions: AMPK is required to coordinate the activation by hypoxia of brainstem respiratory networks and deficiencies in AMPK expression precipitate hypoventilation and apnea, even where carotid body afferent input is normal.

Word count = 246

Keywords: AMP-activated protein kinase; ventilation; apnoea; hypoxia; brainstem.

AJRCCM Articles in Press. Published on 15-December-2015 as 10.1164/rccm.201508-1667OC

AMPK is central to the cell autonomous control of energy supply (1) and comprises a heterotrimer of catalytic α and regulatory β and γ subunits, which are ubiquitously expressed throughout eukaryotes. Under metabolic stresses, such as hypoxia, binding of AMP to one site on the γ subunit and AMP or ADP to another increases AMPK activity, respectively, by allosteric activation and by promoting increased phosphorylation at Thr172 of the α subunit by Liver kinase B1 (2, 3). Alternatively calcium-calmodulin-dependent kinase kinase-β may activate AMPK in response to increases in cytoplasmic calcium (4). AMPK switches off anabolic and switches on catabolic pathways (1), thereby compensating for deficits in ATP supply via, for example, mitochondrial oxidative-phosphorylation. Regulated O_2 supply is key to the maintenance of oxidative phosphorylation and thus cellular energy status in mammals, not least because of the limited capacity for cellular O_2 storage relative to the extensive reserves of other substrates. It was proposed, therefore, that natural selection may have employed AMPK to coordinate whole-body adjustments in response to O_2 deficits in animals (5). Consistent with this view, recent studies on high-altitude, *Andean* populations show that the gene for the AMPK-α1 subunit (*PRKAA1*) has been influenced by natural selection through single nucleotide polymorphisms (6). Moreover tissue-specific changes in AMPK expression occur in metabolic syndrome-related disorders that are associated with sleep-disordered breathing (7, 8).

Ventilatory adjustments are critical to the body's capacity to accommodate variations in O_2 demand and supply during sleep and ascent to altitude, and this is exemplified by the fact that adaptation of mammals to hypoxia at altitude is initially characterized by progressive increases in ventilatory drive that partially restore arterial pO_2 and protect against apnea (9). Ventilatory movements are delivered by respiratory central pattern generators (rCPGs) distributed bilaterally in the pons and ventral medulla. These semi-autonomous neural networks comprise core circuits of excitatory and inhibitory interneurons that deliver rhythmic patterns of activity (10), and confer a set-point about which respiratory rhythm is continuously modulated through the integration of inputs from those central (10, 11) and peripheral chemosensors (12) which monitor O_2, CO_2 and pH. It is generally accepted that the carotid bodies represent the primary

arterial chemoreceptors (12), and that the acute hypoxic ventilatory response (HVR) is delivered by increased afferent discharge from the carotid bodies to the rCPGs via, in great part, catecholaminergic networks within the caudal brainstem (13, 14).

The present study demonstrates conclusively that AMPK deficiency attenuates the HVR and thus precipitates hypoventilation and apnea, by blocking the activation of hypoxia-responsive nuclei within the caudal brainstem (15, 16) even where carotid body afferent inputs are normal. We have previously reported some of these results in the form of an abstract (17).

METHODS

Experiments complied with the regulations of the United Kingdom Animals (Scientific Procedures) Act of 1986.

Breeding of mice, genotyping and single cell PCR

Standard approaches were used (see Supplementary Methods in the online data supplement). All mice studied were between 3-12 months of age.

Computational video analysis of thoracic activity

Thoracic movements were captured by digital camera and the thoracic motion index calculated for each successive frame (see Supplementary Methods in the online data supplement).

Isolated carotid body

Methods for single fiber chemoafferent activity were adapted from those described previously (18); see Supplementary Methods in the online data supplement. Plots of firing frequency versus superfusate pO_2 were fitted by non-linear regression (GraphPad Prism).

Plethysmography

Following 10-20 min acclimation under normoxia (air) mice were exposed to hypoxia (12% or 8% O_2, with 0.05% CO_2, balanced with N_2), or hypoxia+hypercapnia (8% O_2, 5% CO_2, balanced with N_2). Apnea was defined as cessations of breathing greater than the average duration, including interval, of 2

AJRCCM Articles in Press. Published on 15-December-2015 as 10.1164/rccm.201508-1667OC

successive breaths (500ms) during normoxia (19), with a detection threshold of 0.25 mmHg (SD of noise). Breathing variability was assessed by Poincaré plots and by calculating the SD of inter-breath (BB) intervals (19).

Functional magnetic resonance imaging

Mice were anaesthetized (0.8-1.3% isoflurane in air), body temperature maintained (37°C) and breathing frequency monitored by pressure pad sensor. A 7-T horizontal bore MRI scanner (Agilent Technologies, UK), equipped with a high-performance gradient insert (12cm inner diameter, maximum gradient strength 400mT/m) was used. A birdcage coil (72mm diameter) delivered radio frequency transmission, with signal reception via a mouse 2-channel phased array brain coil. All sequences were acquired with: field-of-view 19.2×19.2mm, 30 contiguous coronal slices of 0.4mm thickness.

Structural images were acquired by fast spin echo sequence (train length 8): repetition time (TR) = 3,100ms, effective echo time = 36ms, 8 signal averages, acquisition matrix 192x192, zero-filled to 256x256. Functional images (230 volumes) were acquired during normoxia (21% O_2) and hypoxia (8% O_2) using 3-shot Echo Planar Imaging sequences: repetition time (TR) = 6,000ms (2,000ms per shot), effective echo time = 7.08ms; flip angle 90°, 1 signal average, acquisition matrix 64x64.

Bias corrected (www.slicer.org) structural images were coregistered to a template (www.spmmouse.org) and averaged using SPM8 (Wellcome Trust Centre for Neuroimaging, UCL, UK). Functional data were realigned to mean volumes of each series, spatially normalized (SPM8 co-registration procedures) using each animal's structural scan, and smoothed by 0.7x0.7x4mm full width half maximum (FWHM) Gaussian filter.

For first level analysis see Supplementary Methods in online data supplement. Second-level (group) analysis: The t-map for contrast (*knockout>control*) was thresholded at a level of $P<0.005$ with a 4 voxel cluster threshold (SPM8 imaging software; Wellcome Trust Centre for Neuroimaging, University College London, UK). Between-group differences were analyzed using a region of interest tool. For regions with significant group differences, all voxel signals were averaged at each time point (see also

Supplementary Methods in the online data supplement).

cFos Labelling

Mice were perfused following a single exposure to hypoxia (8% O_2), brain sections incubated in anti-cFos (rabbit; 1:20000 or 100000; Calbiochem) and anti-tyrosine hydroxylase (rat; 1:1000; Millipore) antibodies diluted in blocking buffer, then in biotinylated-anti-rabbit IgG (horse; 1:500; Vector Laboratories) and anti-rat IgG (goat ; 1:750; Invitogen, A594) secondary antibodies (see also Supplementary Methods in the online data supplement).

Statistical analysis

Statistical comparison was completed using GraphPad Prism 6 for the following: *Afferent discharge*, single or 2 factor ANOVA with Bonferroni Dunn post hoc analysis; *Plethysmography*, one-way ANOVA with Bonferroni multiple comparison's test; $P<0.05$ was considered significant. For *fMRI*, a two-sample t-test (SPM8) was used with significance at $P<0.005$.

RESULTS

Loss of AMPK leads to ventilatory dysfunction during hypoxia

Global knockout of both *AMPK-α1* and *-α2* is embryonic lethal. We therefore employed conditional deletion of *AMPK-α1+α2* subunits, using mice in which these genes were flanked by loxP sequences (*α1flx/α2flx* (20)). To direct *AMPK* deletion to catecholaminergic cells of the carotid body (12) and brainstem (21) which contribute to ventilatory control during hypoxia, these were crossed with mice in which Cre recombinase was targeted via the tyrosine hydroxylase (TH) promoter (22). Transient developmental expression of TH occurs in disparate cell groups that do not express TH in the adult (22), including dorsal root ganglion cells, pancreatic islets, a subset of heart wall cells and a subset of gastrointestinal tract cells, none of which contribute to the acute HVR. Therefore, such conditional

AJRCCM Articles in Press. Published on 15-December-2015 as 10.1164/rccm.201508-1667OC

AMPK deletion overcomes embryonic lethality and provides greater discrimination with respect to circuit mechanisms. Cell-specific gene deletion was confirmed by single-cell end-point RT-PCR and whole-brain qPCR (**Figure 1A,B**), and restriction of Cre to TH-positive cells in the adult mouse by viral transfection of a Cre-inducible vector carrying a reporter gene (***see*** **Figure E1** in the online data supplement).

Under normoxia we found no significant difference between *AMPK-α1+α2* knockouts and controls with respect to arterial $sp\mathrm{O}_2$ (***see*** **Figure E2** in the online data supplement), venous blood gases, venous blood pH (***see*** **Table E1** in the online data supplement), weight-gain versus age (***see*** **Figure E3** in the online data supplement), breathing frequency, tidal volume or minute ventilation (***see*** **Figure E4** in the online data supplement). Nevertheless *AMPK* deletion profoundly affected the HVR.

In control mice hypoxia evoked pronounced hyperventilation, characterized by robust increases in minute ventilation (**Figure 1C,D**), breathing frequency and tidal volume (***see*** **Figure E5** in the online data supplement). Dual deletion of *AMPK-α1+α2* markedly attenuated the HVR in response to 12% (mild hypoxia, **Figure 1C**) and 8% O_2 (severe hypoxia, **Figure 1C**), which conferred comparable stimuli in knockouts and controls in terms of the fall in arterial $sp\mathrm{O}_2$ (***see*** **Figure E2** in the online data supplement). Surprisingly, the degree to which the HVR was attenuated increased in a manner directly related to the severity of hypoxia (**Figure 1C,D**), suggesting that AMPK offsets respiratory depression during hypoxia.

Depression of the HVR was most severe upon exposure of *AMPK-α1+α2* knockouts to 8% O_2, which highlights the contribution of AMPK to all phases of the response. For controls, the initial "Augmenting Phase", which is generally accepted to result from increased afferent input from the carotid body, peaked at 106±10% (~30s) relative to normoxia. Following subsequent ventilatory depression (roll off, ~100s) minute ventilation declined to 72±8% above that measured during normoxia, which was maintained for the latter 2-5min of hypoxia (Sustained Phase). For *AMPK-α1+α2* knockouts minute ventilation during the HVR was markedly attenuated compared to controls, measuring, relative to normoxia, only 36±5%

(P<0.0001) during the Augmenting Phase before declining to -4±5% during the Sustained Phase (P<0.0001; 2-5min; 8% O_2); deficits in minute ventilation resulted from reductions in both breathing frequency and tidal volume (***see*** **Figure E5** in the online data supplement). By contrast marked and comparable increases in minute ventilation were evoked upon exposure of controls and knockouts to hypoxia with hypercapnia (8% O_2 + 5% CO_2; **Figure 1C**). Moreover analysis of inter-breath intervals identified greater levels of disordered breathing in *AMPK* knockouts during hypoxia, but not hypercapnic hypoxia, and the severity of disordered breathing increased in a manner directly related to the degree of hypoxia (**Figure 1D-G**).

Hypoxia-evoked *hypoventilation* in *AMPK-α1+α2* knockouts was accompanied by frequent, prolonged apneas (≤6s; **Figure 2 A,B**; ***see also*** **Movie E1-E2** in the online data supplement). Both spontaneous and post-sigh apneas were observed in *AMPK-α1+α2* knockouts (**Figure 2B**) and these resulted from failure of ventilatory drive, which was evident from the absence within ventilatory records of transitions between inspiration and expiration (Personal communication BUXCO/DSI) and confirmed by computational video-analysis of thoracic activity (**Figure 2C**; ***see*** **also Movie E1-E2** in the online data supplement). At 8% O_2 apnea frequency measured 14.3±2.2min^{-1}, apnea duration 953±40ms and apnea duration index (frequency x duration) 13.8±2.2, which were significantly greater (P<0.0001) than measures of apnea frequency (1.8±0.3min^{-1}), apnea duration (709±17ms) and apnea duration index (1.3±0.2) during *hyperventilation* of controls (**Figure 2DI-III**). As might be expected given outcomes for minute ventilation, apnea frequency and duration also increased in a manner directly related to the severity of hypoxia and these increases were completely reversed during hypercapnic hypoxia (**Figure 2D**). Therefore, *AMPK* deletion selectively blocks the HVR and thus precipitates hypoventilation and apnea. Furthermore, because hypercapnic ventilatory drive is retained in these mice and is delivered by CO_2/pH sensitive catecholaminergic neurons (14, 23), it is evident that *AMPK* deletion does not simply block neuronal activation or synaptic transmission *per se* (also see below).

AJRCCM Articles in Press. Published on 15-December-2015 as 10.1164/rccm.201508-1667OC

AMPK is not required for carotid body activation by hypoxia

Surprisingly, reductions in superfusate pO_2 raised chemoafferent discharge exponentially in all carotid bodies (**Figure 3A,B**), with peak discharge frequency at a pO_2 of ~74 mmHg measuring 12.5±1.6Hz (n=10) for controls and 13.9±1.5Hz (n=8; P<0.001) for *AMPK-α1+α2* knockouts. Therefore, AMPK is not required for carotid body activation during hypoxia and *AMPK* deletion does not compromise either exocytosis in or subsequent synaptic transmission by TH-expressing cells. Hence *AMPK* deletion must block the HVR by attenuating activation of the hypoxia-responsive respiratory network at a point distal to the carotid body.

AMPK deletion markedly attenuates activation of brainstem nuclei by hypoxia

Catecholaminergic and other neurons of the nucleus tractus solitarius (NTS) and ventrolateral medulla receive inputs from the carotid body (21, 24, 25), are activated by CNS hypoxia and may independently regulate rCPGs in a manner dependent on continued basal (normoxic) afferent input from the carotid bodies (13, 16, 26). Brainstem activity during hypoxia was therefore assessed by functional magnetic resonance imaging (fMRI) in anaesthetized mice, in light of the fact that ≤9% O_2 induces cerebral vasodilation sufficient to eliminate the BOLD signal driven, under normoxia, by increases in cerebral blood flow in response to sensory stimulation (27). This allowed analysis of regional differences in signal change resulting from reductions in O_2-consumption (decreased BOLD signal) in *AMPK-α1+α2* knockouts, relative to controls, during acute exposure to 8% O_2 (2 min; ~40% *sp*O2). Second level (group) fMRI analysis during hypoxia identified significantly different BOLD signals in two well-defined dorsal (DAR) and ventral (VAR) active regions of the caudal brainstem of all *AMPK-α1+α2* knockouts when compared to controls (**Figure 4C,D**). Signal change for the DAR measured -23.58±1.17 in controls and -14.93±0.91 (P<0.01) in *AMPK-α1+α2* knockouts (**Figure 4E**), and, respectively, -11.78±0.91 and -8.3±0.37 for the VAR (P<0.05). The DAR and VAR exhibited pronounced right-left asymmetry, although removing the 4-voxel cluster threshold revealed limited

evidence of right-side-dominant, bilateral symmetry for the VAR alone (***see*** **Figure E6** in the online data supplement). Hypoxia (8% O_2) evoked concomitant ***increases*** in breathing frequency of +16.54±12.92 breaths min^{-1} in controls (n = 5; **Figure 4 A,B**). By contrast all *AMPK-α1+α2* knockouts exhibited concomitant ***decreases*** in breathing frequency of -59.80±1.75 breaths min^{-1} (n = 6, P<0.001; **Figure 4 A,B**). Furthermore, anesthesia sufficient to lower breathing frequency of *AMPK-α1+α2* knockouts below 90 breaths min^{-1} precipitated irreversible respiratory failure within 30s of hypoxia (n=4; excluded from fMRI analysis). Therefore, anesthesia exacerbates hypoxic respiratory depression in *AMPK-α1+α2* knockouts.

The caudal location relative to Bregma of the DAR (**Figure 4C**) is consistent with that of the NTS, within which poorly defined subgroups of A2 catecholaminergic neurons receive carotid body afferent inputs (24) and are activated during hypoxia (16, 21). The location of the VAR aligns well with the C1/A1 catecholaminergic neurons of the ventrolateral medulla, which are activated during hypoxia via afferent inputs from both carotid bodies and the NTS (21, 28, 29). We therefore used immediate early gene expression (*cfos*), the only truly physiological approach available (13, 21), to identify the subpopulation(s) of cells within the brainstem of *AMPK-α1+α2* knockouts that exhibit deficits in activity during hypoxia *in-vivo*. Cell counts revealed no deficit in TH-positive cells across any of the regions studied (not shown). Regardless, *AMPK* deletion selectively attenuated hypoxia-evoked (8% O_2) increases in *cfos* expression in cells adjacent to the area postrema (SubP) and within the medial subnucleus (SolM; **Figure 5A *lefthand panel***). The SubP of controls contained 1.09±0.56 TH-positive and cFos-positive cells/100μm^2 and 0.79±0.21 cFos-positive and TH-negative cells/100μm^2, which fell in *AMPK-α1+α2* knockouts to, respectively, 0.27±0.1 cells/100μm^2 (p<0.01) and 0.28±0.1 cells/100μm^2 (p<0.01; **Figure 5B**). In SolM, however, a reduction in *cfos* expression was only observed in TH-negative cells, from 1.91±0.3 cells/100μm^2 in controls to 1.16±0.27 cells/100μm^2 (p<0.05) in *AMPK-α1+α2* double knockouts (**Figure 5B**). By contrast, a small but significant increase in the number of

AJRCCM Articles in Press. Published on 15-December-2015 as 10.1164/rccm.201508-1667OC

cFos positive cells was observed in TH-positive neurons within the SolC, ventral and ventrolateral A2 regions (**Figure 5B**). Rostral to these A2 nuclei, a significant reduction in *cfos* expression was also observed in all dorsal C2 neurons (**Figure 5A,B**), from 6.75±0.62 to 5.4±0.44 TH-positive cells/100μm^2 ($p<0.05$) and from 0.78±0.20 to 0.23±0.1 TH-negative cells/100μm^2 ($p<0.05$).

Ventral A1 regions of *AMPK-α1+α2* knockouts, proximal to the VAR identified by fMRI, exhibited selective reductions of *cfos* expression in TH-positive, but not TH-negative, cells, from 4.66±0.26 to 3.88±0.23 cells/100μm^2 ($p<0.05$, **Figure 5A,B**). By contrast, *AMPK* deletion increased the number *cfos* expressing, TH-positive cells within the C1 region after hypoxia, from 5.05±0.21 to 6.29±0.30 cells/100μm^2 ($p<0.05$, **Figure 5A,B**).

These data suggest differential AMPK-dependency of the activation during hypoxia of dorsal and ventral brainstem nuclei known to contribute to the HVR. Although we can't rule out the possibility of confounding developmental abnormalities associated with *AMPK* deletion, we observe no deficits in ventilatory function during normoxia or hypercapnic hypoxia, no obvious structural anomaly by fMRI and no deficit in TH-positive or TH-negative cell count within the brainstem of *AMPK-α1+α2* double knockouts.

Loss of AMPK-α1 subunit expression is the primary cause of ventilatory dysfunction during hypoxia

Figure 6 compares exemplar Poincaré plots of inter-breath interval (BBn) versus subsequent inter-breath interval (BBn+1) during (**AI**) normoxia and (**BI**) hypoxia for controls and knockouts of *AMPK-α2*, *AMPK-α1* and *AMPK-α1+α2*. During hypoxia, while inter-breath intervals of *AMPK-α2* knockouts were similar to controls, breathing irregularities resulted from *AMPK-α1* deletion and these increased in severity with deletion of *AMPK-α1+α2*. Confirmation was provided by comparison of the SD of inter-breath intervals (**Figure 6AII,BII**), which increased from 167±24ms during hypoxia with *AMPK-α1*

deletion to 238±23ms with deletion of *AMPK-α1+α2* (P<0.001). Likewise, comparison of apnea duration index (**Figure 6C**) and minute ventilation (**Figure 6D**) demonstrated that ventilatory dysfunction was primarily driven by loss of *AMPK-α1*, but was more severe for *AMPK-α1+α2* deletion. Hence AMPK-α2 containing heterotrimers confer only marginal compensation for loss of AMPK-α1.

DISCUSSION

Deficiencies of *AMPK* expression precipitated ventilatory dysfunction during hypoxia, characterized by marked hypoventilation, rather than hyperventilation, and frequent, prolonged apneas. Upon hypoxia at altitude or during sleep, AMPK activation may therefore support hyperventilation and thus 'protect' against hypoxia-induced ventilatory instability (9), while AMPK deficiency may confer greater susceptibility to disordered breathing. That loss of *AMPK-α1* was the primary precipitant is notable in this respect, given that natural selection in high-altitude (*Andean*) populations has led to single nucleotide polymorphisms in *PRKAA1*, the gene for AMPK-α1 (6).

Against expectations, however, *AMPK* deletion failed to attenuate hypoxia-evoked afferent discharge from the carotid body. This is contrary to our previous pharmacological studies which suggested that AMPK activation by hypoxia might elicit type I cell exocytosis and increase afferent discharge (18), but is consistent with more recent investigations (30). Previous conflicting observations may have arisen due to off target effects of pharmacological tools, such as AICAR-mediated reductions in the adenylate pool and ATP (20, 31). Regardless, AMPK is clearly not necessary for carotid body activation by hypoxia. Given that *AMPK* deletion blocked the HVR, this may appear contrary to the view that increased afferent discharge from the carotid body to the brainstem determines the ventilatory response to a fall in arterial pO_2 (12). However, evidence suggests that the HVR is determined by the coordinated action of the carotid body and a hypoxia-responsive circuit within the brainstem (26) comprising, in great part, TH-expressing catecholaminergic cells (14, 15).

Consistent with this view, fMRI analysis identified that *AMPK* deletion markedly attenuated activation

AJRCCM Articles in Press. Published on 15-December-2015 as 10.1164/rccm.201508-1667OC

by hypoxia of dorsal and ventral nuclei of the caudal brainstem, even though carotid body afferent discharge was retained, and this was corroborated by analysis of *cfos* expression. The caudal location relative to Bregma of the dorsal active region is consistent with areas of the NTS that are activated by hypoxia and which represent the primary site of receipt of carotid body afferent input (13, 16, 24). Here *AMPK* deletion selectively attenuated *cfos* expression during hypoxia by mixed subpopulations of C2 neurons and A2 neurons (SubP; SolM) within the medial subnucleus proximal to the midline and the area postrema, which are activated during hypoxia (21). A2 neurons of the NTS provide afferent input to and determine, together with the carotid body, activation by hypoxia of A1/C1 neurons within the ventrolateral medulla (21, 28), the position of which (28) aligns well with the ventral active region identified by fMRI analysis; by contrast projections of the NTS mostly avoid (28) the Bötzinger and pre-Bötzinger complexes (32). *AMPK* deletion selectively reduced *cfos* expression by TH-positive A1 neurons during hypoxia. This may be significant given that carotid body afferent input alone is sufficient to activate C1 neurons and thus elicits hypotension (29), which was likewise induced by hypoxia in *AMPK* knockouts and controls. Our findings therefore suggest that respiratory input from the carotid chemoreflex may be blocked by loss of AMPK function within a neuronal circuit spanning the C2/A2 neurons of the NTS and the A1 neurons of the ventrolateral medulla, which opposes respiratory depression during hypoxia. This is consistent with optogenetic and pharmacological interventions at the NTS (16, 33), and the proposal that NTS neurons lie on the sensory side of the central respiratory network (34, 35). Observed right-left asymmetry of brainstem activation during hypoxia (**Figure 4**) may provide for specialization sufficient to prevent delays in respiratory responses to hypoxic stress, by limiting conflicting outputs from each side of the brain (36) as for cognitive performance (37). Furthermore and despite the fact that cell counts were not biased by considerations on right-left asymmetry of brainstem activation, observed changes in *cfos* expression suggest that AMPK deficiency attenuates the activation by hypoxia of a discrete subpopulation of respiratory neurons within the C2, A2 and A1 nuclei; which may also explain, in part, the modest deficits in *cfos* expression of *AMPK*

knockouts relative to the ventilatory dysfunction observed. In this respect it is notable that C2 and A2 neurons are both catecholaminergic and glutamatergic (34, 38), and that 6-10% of TH-positive C2, A2 and A1 neurons also express neuronal nitric oxide synthase, which supports the HVR by synthesizing NO (39) and/or *S*-nitrosothiols (40), and in a manner that may be facilitated by AMPK (41). However further investigation will be required to determine how right-left asymmetry is orchestrated by AMPK and the complex interplay of those neurotransmitters deployed during hypoxia.

AMPK deletion in catecholaminergic cells may simply lead to the failure of central integration and transduction of peripheral chemoafferent input and consequent failure of the HVR, due to the inability of affected neurons to respond appropriately to metabolic stress (42). However, given that carotid body afferent discharge remains exquisitely sensitive to a fall in pO_2 and ventilatory responses to hypercapnia remain unaffected even during severe (8%) hypoxia, our data demonstrate that *AMPK* deletion does not compromise, *per se*, the capacity during hypoxia for activation of chemosensory catecholaminergic neurons, exocytosis nor effective delivery of increased respiratory drive. This is consistent with the observation that neuronal integrity during hypoxia may be preserved, in part, by AMPK-independent mechanisms (43) that maintain ATP supply by accelerating glycolysis and in a manner supported by mobilization of astrocyte glycogen stores (44). That said, we must also consider why: 1) The degree of block by *AMPK* deletion of the HVR increased in a manner directly related to the severity of hypoxia; 2) The HVR can be triggered by CNS hypoxia alone, providing there is continued receipt of basal (normoxic) afferent input from the carotid bodies (26); 3) Interference at any point within this circuit abolishes the HVR, e.g., carotid body resection (45) or AMPK deletion. We therefore hypothesize that AMPK signaling pathways support coincidence detection at a point of signal integration within and thus activation of a hypoxia-responsive circuit that encompasses C2/A2 neurons and ventrolateral A1 neurons. We envisage that coincidence detection is delivered by the capacity for AMPK activation by increases in AM(D)P/ATP ratio (1) determined by "local hypoxic stress" within the NTS (decreased ATP supply), which is coupled with "applied metabolic stress" (increased ATP usage) and/or increased

AJRCCM Articles in Press. Published on 15-December-2015 as 10.1164/rccm.201508-1667OC

cytoplasmic Ca^{2+} delivered via afferent input from the carotid bodies to the NTS and, in turn, to ventrolateral A1 neurons (**Figure 7**). Afferent input and brainstem hypoxia could thereby determine, each in part, the set-point about which AMPK and thus the brainstem respiratory network are activated during hypoxia. Thereafter, AMPK-dependent modulation of cellular metabolism (1), ion channels and thus neuronal firing frequency (46) and / or transmitter release (40, 41) may facilitate efferent output and thus deliver increased drive to breathe, in a manner that may be attenuated or augmented by appropriate regulation of *AMPK* expression.

It is also noteworthy that *AMPK* knockout mice not only hypoventilate during hypoxia, but also lie down and appear to enter a "torpor-like" state from which they recover rapidly when returned to normoxia (***see*** **Movie E1-E2** in the online data supplement). These mice may therefore engage alternative strategies to reduce O_2 consumption and maintain supply, perhaps by entering a hypometabolic state (47). This would explain the comparable arterial $sp O_2$ for controls and *AMPK* knockouts during hypoxia, despite the attenuated HVR of the latter.

During anesthesia, loss of suprapontine (voluntary) control of ventilation (48) may have exacerbated hypoxic ventilatory depression in *AMPK* knockouts and perhaps revealed the true extent of deficiencies in brainstem respiratory drive during hypoxia, which in the extreme precipitated death by irreversible respiratory failure. Interestingly, such outcomes are consistent with the effect of anesthesia on patients suffering from sleep apnea (49). Moreover observed respiratory failure could be triggered by exacerbation of the Cushing reflex (13, 50), although this is only elicited under anesthesia by ischemic hypoxia (~1% O_2) and is maintained or enhanced by hypercapnia (13, 50, 51). By contrast, hypoxic ventilatory depression was evident in conscious *AMPK* knockouts during mild and severe hypoxia, as were deficits in brainstem activity, and was reversed rather than exacerbated by hypercapnia. Furthermore and contrary to the marked increases in blood pressure associated with the Cushing reflex (13, 50), hypoxic ventilatory depression in *AMPK* knockouts was associated with a fall in blood pressure equivalent to controls (***see*** **Figure E7** in the online data supplement) and wild-type mice (52).

Notwithstanding these facts, hypoxia triggers increased blood pressure in both rats (53) and humans (54) and we cannot rule out the possibility that outcomes for blood pressure may reflect species-dependent variations allied to the Cushing reflex (50).

We conclude that AMPK opposes central respiratory depression during hypoxia and resists hypoventilation and apnea by supporting increases in central respiratory drive, even where carotid body afferent input is normal. Consequently, AMPK deficiency precipitates ventilatory dysfunction during hypoxia. AMPK is therefore key to O_2 and thus energy (ATP) supply to the body as a whole. Moreover modulation of AMPK activity or expression may afford new therapeutic strategies against hypoventilation and apnea associated, for example, with metabolic syndrome-related disorders and ascent to altitude (7-9).

AJRCCM Articles in Press. Published on 15-December-2015 as 10.1164/rccm.201508-1667OC

REFERENCES

1. Hardie DG. AMPK-sensing energy while talking to other signaling pathways. *Cell Metab* 2014; 20: 939-952.
2. Gowans GJ, Hawley SA, Ross FA, Hardie DG. AMP is a true physiological regulator of AMP-activated protein kinase by both allosteric activation and enhancing net phosphorylation. *Cell Metabolism* 2013; 18: 556-566.
3. Sakamoto K, McCarthy A, Smith D, Green KA, Grahame Hardie D, Ashworth A, Alessi DR. Deficiency of LKB1 in skeletal muscle prevents AMPK activation and glucose uptake during contraction. *EMBO J* 2005; 24: 1810-1820.
4. Woods A, Dickerson K, Heath R, Hong SP, Momcilovic M, Johnstone SR, Carlson M, Carling D. Ca^{2+}/calmodulin-dependent protein kinase kinase-beta acts upstream of AMP-activated protein kinase in mammalian cells. *Cell Metabolism* 2005; 2: 21-33.
5. Evans AM. AMP-activated protein kinase and the regulation of Ca^{2+} signalling in O_2-sensing cells. *J Physiol* 2006; 574: 113-123.
6. Bigham AW, Julian CG, Wilson MJ, Vargas E, Browne VA, Shriver MD, Moore LG. Maternal PRKAA1 and EDNRA genotypes are associated with birth weight, and PRKAA1 with uterine artery diameter and metabolic homeostasis at high altitude. *Physiol Genomics* 2014; 46: 687-697.
7. Ruderman NB, Carling D, Prentki M, Cacicedo JM. AMPK, insulin resistance, and the metabolic syndrome. *J Clin Invest* 2013; 123: 2764-2772.
8. Chau EH, Lam D, Wong J, Mokhlesi B, Chung F. Obesity hypoventilation syndrome: a review of epidemiology, pathophysiology, and perioperative considerations. *Anesthesiology* 2012; 117: 188-205.
9. Ainslie PN, Lucas SJ, Burgess KR. Breathing and sleep at high altitude. *Respir Physiol Neurobiol* 2013; 188: 233-256.
10. Smith JC, Abdala AP, Borgmann A, Rybak IA, Paton JF. Brainstem respiratory networks: building blocks and microcircuits. *Trends Neurosci* 2013; 36: 152-162.
11. Day TA, Wilson RJ. Brainstem PCO_2 modulates phrenic responses to specific carotid body hypoxia in an in situ dual perfused rat preparation. *J Physiol* 2007; 578: 843-857.
12. Nurse CA. Synaptic and paracrine mechanisms at carotid body arterial chemoreceptors. *J Physiol* 2014; 592: 3419-3426.
13. Guyenet PG. Neural structures that mediate sympathoexcitation during hypoxia. *Respir Physiol* 2000; 121: 147-162.
14. Guyenet PG. Regulation of breathing and autonomic outflows by chemoreceptors. *Compr Physiol* 2014; 4: 1511-1562.
15. Sun MK, Reis DJ. Differential responses of barosensitive neurons of rostral ventrolateral medulla to hypoxia in rats. *Brain Res* 1993; 609: 333-337.
16. King TL, Heesch CM, Clark CG, Kline DD, Hasser EM. Hypoxia activates nucleus tractus solitarii neurons projecting to the paraventricular nucleus of the hypothalamus. *Am J Physiol Regul Integr Comp Physiol* 2012; 302: R1219-1232.
17. Mahmoud AD, Lewis S, Juričić L, Foretz M, Viollet B, Marshall I, Evans AM. AMPK couples oxygen to energy supply at the whole-body level by delivering increased drive to breathe during hypoxia and thus protects against apnoea (Paper presented at the annual meeting of the Physiological Society, Cardiff, UK, July 6-8, 2015). *Proc Physiol Soc* 2015; 34: PC041.
18. Wyatt CN, Mustard KJ, Pearson SA, Dallas ML, Atkinson L, Kumar P, Peers C, Hardie DG, Evans AM. AMP-activated protein kinase mediates carotid body excitation by hypoxia. *J Biol Chem* 2007; 282: 8092-8098.

19. Peng YJ, Nanduri J, Khan SA, Yuan G, Wang N, Kinsman B, Vaddi DR, Kumar GK, Garcia JA, Semenza GL, Prabhakar NR. Hypoxia-inducible factor 2alpha (HIF-2alpha) heterozygous-null mice exhibit exaggerated carotid body sensitivity to hypoxia, breathing instability, and hypertension. *Proc Natl Acad Sci U S A* 2011; 108: 3065-3070.
20. Lantier L, Fentz J, Mounier R, Leclerc J, Treebak JT, Pehmoller C, Sanz N, Sakakibara I, Saint-Amand E, Rimbaud S, Maire P, Marette A, Ventura-Clapier R, Ferry A, Wojtaszewski JF, Foretz M, Viollet B. AMPK controls exercise endurance, mitochondrial oxidative capacity, and skeletal muscle integrity. *FASEB J* 2014; 28: 3211-3224.
21. Hirooka Y, Polson JW, Potts PD, Dampney RA. Hypoxia-induced Fos expression in neurons projecting to the pressor region in the rostral ventrolateral medulla. *Neuroscience* 1997; 80: 1209-1224.
22. Lindeberg J, Usoskin D, Bengtsson H, Gustafsson A, Kylberg A, Soderstrom S, Ebendal T. Transgenic expression of Cre recombinase from the tyrosine hydroxylase locus. *Genesis* 2004; 40: 67-73.
23. Kumar NN, Velic A, Soliz J, Shi Y, Li K, Wang S, Weaver JL, Sen J, Abbott SB, Lazarenko RM, Ludwig MG, Perez-Reyes E, Mohebbi N, Bettoni C, Gassmann M, Suply T, Seuwen K, Guyenet PG, Wagner CA, Bayliss DA. Regulation of breathing by CO_2 requires the proton-activated receptor GPR4 in retrotrapezoid nucleus neurons. *Science* 2015; 348: 1255-1260.
24. Koshiya N, Guyenet PG. NTS neurons with carotid chemoreceptor inputs arborize in the rostral ventrolateral medulla. *Am J Physiol* 1996; 270: R1273-1278.
25. Erickson JT, Millhorn DE. Hypoxia and electrical stimulation of the carotid sinus nerve induce Fos-like immunoreactivity within catecholaminergic and serotoninergic neurons of the rat brainstem. *J Comp Neurol* 1994; 348: 161-182.
26. Smith CA, Forster HV, Blain GM, Dempsey JA. An interdependent model of central/peripheral chemoreception: evidence and implications for ventilatory control. *Respir Physiol Neurobiol* 2010; 173: 288-297.
27. Sicard KM, Duong TQ. Effects of hypoxia, hyperoxia, and hypercapnia on baseline and stimulus-evoked BOLD, CBF, and CMRO2 in spontaneously breathing animals. *Neuroimage* 2005; 25: 850-858.
28. Alheid GF, Jiao W, McCrimmon DR. Caudal nuclei of the rat nucleus of the solitary tract differentially innervate respiratory compartments within the ventrolateral medulla. *Neuroscience* 2011; 190: 207-227.
29. Abbott SB, Depuy SD, Nguyen T, Coates MB, Stornetta RL, Guyenet PG. Selective optogenetic activation of rostral ventrolateral medullary catecholaminergic neurons produces cardiorespiratory stimulation in conscious mice. *J Neurosci* 2013; 33: 3164-3177.
30. Kim D, Kang D, Martin EA, Kim I, Carroll JL. Effects of modulators of AMP-activated protein kinase on TASK-1/3 and intracellular Ca^{2+} concentration in rat carotid body glomus cells. *Respir Physiol Neurobiol* 2014; 195: 19-26.
31. Hasenour CM, Ridley DE, Hughey CC, James FD, Donahue EP, Shearer J, Viollet B, Foretz M, Wasserman DH. 5-Aminoimidazole-4-carboxamide-1-beta-D-ribofuranoside (AICAR) effect on glucose production, but not energy metabolism, is independent of hepatic AMPK in vivo. *J Biol Chem* 2014; 289: 5950-5959.
32. Smith JC, Ellenberger HH, Ballanyi K, Richter DW, Feldman JL. Pre-Botzinger complex: a brainstem region that may generate respiratory rhythm in mammals. *Science* 1991; 254: 726-729.
33. Yamamoto K, Lalley P, Mifflin S. Acute intermittent optogenetic stimulation of nucleus tractus solitarius neurons induces sympathetic long-term facilitation. *Am J Physiol Regul Integr Comp Physiol* 2015; 308: R266-275.
34. Vardhan A, Kachroo A, Sapru HN. Excitatory amino acid receptors in commissural nucleus of the NTS mediate carotid chemoreceptor responses. *Am J Physiol* 1993; 264: R41-50.

AJRCCM Articles in Press. Published on 15-December-2015 as 10.1164/rccm.201508-1667OC

35. Aicher SA, Saravay RH, Cravo S, Jeske I, Morrison SF, Reis DJ, Milner TA. Monosynaptic projections from the nucleus tractus solitarii to C1 adrenergic neurons in the rostral ventrolateral medulla: comparison with input from the caudal ventrolateral medulla. *J Comp Neurol* 1996; 373: 62-75.
36. Vallortigara G, Rogers LJ, Bisazza A. Possible evolutionary origins of cognitive brain lateralization. *Brain Res Rev* 1999; 30: 164-175.
37. Dadda M, Zandona E, Agrillo C, Bisazza A. The costs of hemispheric specialization in a fish. *Proc Biol Sci* 2009; 276: 4399-4407.
38. Stornetta RL, Sevigny CP, Guyenet PG. Vesicular glutamate transporter DNPI/VGLUT2 mRNA is present in C1 and several other groups of brainstem catecholaminergic neurons. *J Comp Neurol* 2002; 444: 191-206.
39. Gozal D, Gozal E, Torres JE, Gozal YM, Nuckton TJ, Hornby PJ. Nitric oxide modulates ventilatory responses to hypoxia in the developing rat. *Am J Respir Crit Care Med* 1997; 155: 1755-1762.
40. Lipton AJ, Johnson MA, Macdonald T, Lieberman MW, Gozal D, Gaston B. S-nitrosothiols signal the ventilatory response to hypoxia. *Nature* 2001; 413: 171-174.
41. Murphy BA, Fakira KA, Song Z, Beuve A, Routh VH. AMP-activated protein kinase and nitric oxide regulate the glucose sensitivity of ventromedial hypothalamic glucose-inhibited neurons. *Am J Physiol Cell Physiol* 2009; 297: C750-758.
42. Culmsee C, Monnig J, Kemp BE, Mattson MP. AMP-activated protein kinase is highly expressed in neurons in the developing rat brain and promotes neuronal survival following glucose deprivation. *J Mol Neurosci* 2001; 17: 45-58.
43. Cheng F, Xie S, Guo M, Fang H, Li X, Yin J, Lu G, Li Y, Ji X, Yu S. Altered glucose metabolism and preserved energy charge and neuronal structures in the brain of mouse intermittently exposed to hypoxia. *J Chem Neuroanat* 2011; 42: 65-71.
44. Almeida A, Moncada S, Bolanos JP. Nitric oxide switches on glycolysis through the AMP protein kinase and 6-phosphofructo-2-kinase pathway. *Nat Cell Biol* 2004; 6: 45-51.
45. Wade JG, Larson CP, Jr., Hickey RF, Ehrenfeld WK, Severinghaus JW. Effect of carotid endarterectomy on carotid chemoreceptor and baroreceptor function in man. *N Engl J Med* 1970; 282: 823-829.
46. Ikematsu N, Dallas ML, Ross FA, Lewis RW, Rafferty JN, David JA, Suman R, Peers C, Hardie DG, Evans AM. Phosphorylation of the voltage-gated potassium channel Kv2.1 by AMP-activated protein kinase regulates membrane excitability. *Proceedings of the National Academy of Sciences* 2011; 108: 18132-18137.
47. Guppy M, Withers P. Metabolic depression in animals: physiological perspectives and biochemical generalizations. *Biol Rev Camb Philos Soc* 1999; 74: 1-40.
48. Horn EM, Waldrop TG. Suprapontine control of respiration. *Respir Physiol* 1998; 114: 201-211.
49. Boushra NN. Anaesthetic management of patients with sleep apnoea syndrome. *Can J Anaesth* 1996; 43: 599-616.
50. Paton JF, Dickinson CJ, Mitchell G. Harvey Cushing and the regulation of blood pressure in giraffe, rat and man: introducing 'Cushing's mechanism'. *Exp Physiol* 2009; 94: 11-17.
51. Harris AP, Helou S, Traystman RJ, Jones MD, Jr., Koehler RC. Efficacy of the cushing response in maintaining cerebral blood flow in premature and near-term fetal sheep. *Pediatr Res* 1998; 43: 50-56.
52. Campen MJ, Shimoda LA, O'Donnell CP. Acute and chronic cardiovascular effects of intermittent hypoxia in C57BL/6J mice. *J Appl Physiol (1985)* 2005; 99: 2028-2035.
53. Bakehe M, Hedner J, Dang T, Chambille B, Gaultier CL, Escourrou P. Role of the autonomic nervous system in the acute blood pressure elevation during repetitive hypoxic and hypercapnic breathing in rats. *Blood Press* 1996; 5: 371-375.

54. Somers VK, Mark AL, Zavala DC, Abboud FM. Contrasting effects of hypoxia and hypercapnia on ventilation and sympathetic activity in humans. *J Appl Physiol (1985)* 1989; 67: 2101-2106.

FIGURE LEGENDS

Figure 1. Conditional deletion of *AMPK* catalytic α-subunits in tyrosine hydroxylase expressing cells markedly attenuates the hypoxic ventilatory response. (*A*) Single cell end-point RT-PCR amplicons for tyrosine hydroxylase and the catalytic α1 and α2 subunits of AMPK from acutely isolated carotid body type I cells of wild type **(**WT CB1 cells**)** and *AMPK-α1* and *-α2* double knockout mice **(***AMPK* Double KO CB1 cells**)**. (*B*) q-RT-PCR assays of AMPK-α1 and -α2 subunit expression of mouse brain as a % of β-actin from mice wild type (WT) and *AMPK-α1* and *-α2* double knockout mice (n=3). (*C*), *Upper panels* show example records of minute ventilation (ml min^{-1} g^{-1}) versus time during 12% O_2, 8% O_2 and 8% O_2 with 5% CO_2 for *AMPK-α1* and *-α2* double floxed (*AMPK* Double FX, black, n = 31) and *AMPK-α1* and *-α2* double knockout mice (*AMPK* Double KO, red, n = 22). *Lower panels*, Bar charts show mean±SEM for increase in minute ventilation for the peak of the Augmenting Phase (A), after 100s of Roll Off (RO) and the plateau of the Sustained Phase (SP) of the response to hypoxia; ****=p<0.0001. (*D-F*) show exemplar Poincaré plots of the inter-breath interval (BBn) versus subsequent interval (BBn+1) of *AMPK-α1 and -α2* double floxed (*AMPK* Double FX, black), and *AMPK-α1* and *-α2* double knockout (*AMPK* Double KO, red) mice during: (*D*) Mild hypoxia (12% O_2 + 0.05% CO_2); (*E*) Severe hypoxia (8% O_2 + 0.05% CO_2); (*F*) hypoxia with hypercapnia (8% O_2 + 5% CO_2). (*G*) Shows corresponding mean ± SEM for the standard deviation (SD) of BBn and BBn+1 for each genotype during 12% O_2 (*AMPK* double FX, n = 31; *AMPK* double KO, n = 22), 8% O_2 + 0.05%

AJRCCM Articles in Press. Published on 15-December-2015 as 10.1164/rccm.201508-1667OC

CO_2 (*AMPK* Double FX, n = 12; *AMPK* Double KO, n = 19) and 8% O_2 + 5% CO_2 (*AMPK* Double FX, n = 20; *AMPK* Double KO, n = 29); *** =P<0.001, **** = p < 0.0001.

Figure 2. Deletion of *AMPK* precipitates hypoventilation and apnea. (*A*) Records of ventilatory activity obtained using whole body plethysmography from *AMPK* Double FX (n = 31) and *AMPK* Double KO (n = 22) mice during (*I*) normoxia (21% O_2), (*II*) hypoxia (8% O_2) and (*III*) hypoxia with hypercapnia (8% O_2 + 5% CO_2). (*BI-II*) Typical ventilatory records on an expanded time scale during hypoxia (8% O_2). (*CI-II*), Computational video analysis of thoracic movement (*upper panels*) with corresponding ventilatory traces (*lower panels*). (*D*) mean±SEM for (*I*) apneic index (per minute), (*II*) apnea duration (s) and (*III*) apnea-duration index (frequency x duration); (*AMPK* Double FX, n = 31; *AMPK* Double KO, n = 22) *=p<0.05, **=p<0.01, *** =P<0.001, ****=p< 0.0001.

Figure 3. *AMPK* deletion does not inhibit carotid body activation by hypoxia. *Upper panels* show extracellular recordings of single fiber chemoafferent discharge vs pO_2 for (*A*) *AMPK-α1* and -α2 *double floxed (AMPK* Double FX) and (*B*) *AMPK-α1* and -α2 double knockouts (*AMPK* Double KO); inset, single fiber discriminations. *Middle*, frequency-time histograms. *Lower*, frequency-pO_2 response curves.

Figure 4. Functional magnetic resonance imaging demonstrates that *AMPK* deletion inhibits activation by hypoxia of dorsal and ventral regions of the brainstem. (*A*) Example records of frequency (breaths min^{-1}) versus time during hypoxia (8% O_2) for anaesthetized *AMPK-α1* and *-α2* double floxed (*AMPK* Double FX, black, n = 6) and *AMPK-α1* and *-α2* double knockout mice (*AMPK* Double KO, red, n = 6). (*B*) Bar charts show mean±SEM for change in breathing frequency during hypoxia; **=p< 0.01. (*C*) Dorsal (DAR) and ventral (VAR) active regions of brainstem that exhibited significantly lower signal change (p<0.005) during hypoxia in *AMPK* Double KO when compared to Double FX control mice. (*D*) Variability of signal time courses for DAR and VAR in blue for each

individual mouse (same mice as for A, lower panel) overlaid on mean signal for *AMPK* Double FX (black line) and *AMPK* Double KO (red line); AU = arbitrary units. (*E*) mean±SEM percentage signal changes for DAR and VAR during hypoxia (same mice as for A, lower panel). *=p< 0.05, **=p< 0.01.

Figure 5. AMPK deletion attenuates cFOS expression in discrete areas of the NTS and ventrolateral medulla. (*A*) Immunostaining of a brainstem section derived from an *AMPK-α1* and *-α2* double knockout mouse, shows cfos (green) and Tyrosine Hydroxylase (TH, red) staining in the A2 and C2 regions of the nucleus of the solitary tract, and the ventrolateral C1/A1 region. Abbreviations: AP, area postrema; SubP, SolC, SolM, SolIM, SolDL, SolV, SolVL: Sub Postrema, commissural, medial, intermediate, dorsolateral, ventral and ventrolateral regions of the nucleus of the solitary tract; CC, central canal; IV, fourth ventricle; X, dorsal motor nucleus of the vagus; XII, hypoglossal nucleus. Scale bar 50 μm. (*B*) Bar charts show for each region in (*A*) the number of TH-positive and TH-negative cells per 1000 μm^2 in which cfos expression increased during hypoxia (8%O_2) for *AMPK-α1* and *-α2* double floxed (*AMPK* Double FX, black, n = 19 sections, n = 6 mice) and *AMPK-α1* and *-α2* double knockout mice (*AMPK* Double KO, red, n = 17 sections, n = 6 mice). *=p< 0.01.

Figure 6. Respiratory dysfunction during hypoxia is primarily mediated by loss of the AMPK-α1 subunit. Exemplar Poincaré plots of the inter-breath interval (BB_n) versus subsequent interval (BB_{n+1}) for mice with *AMPK-α1* and *-α2* floxed (*AMPK* Double FX, n=31), *AMPK-α2* knockout (*AMPK-α2* KO, n=16), *AMPK-α1* knockout (*AMPK-α*1 KO, n=19), and *AMPK-α1* and *-α2* double knockout (*AMPK* Double KO, n=22) during: (*AI*) normoxia (21% O_2); (*BII*) hypoxia (8% O_2). (*AII-BII*) Corresponding mean±SEM for the standard deviation (SD) of BB_n and BB_{n+1} for each genotype under normoxia and 8% O_2. (*C*) mean±SEM for (*I*) apnoeic index (per minute), (*II*) apnea duration (s) and (*III*) apnea-duration index. (*D*) Increases in minute ventilation relative to normoxia at Augmenting Phase (**A**), after 100s of

AJRCCM Articles in Press. Published on 15-December-2015 as 10.1164/rccm.201508-1667OC

Roll Off (**RO**) and the plateau of the Sustained Phase (**SP**) of the response to hypoxia; *=p<0.05, **=p<0.01, *** =P<0.001, ****=p< 0.0001.

Figure 7. Schematic describes the new hypothesis on the integration by AMPK of local and applied metabolic stresses.

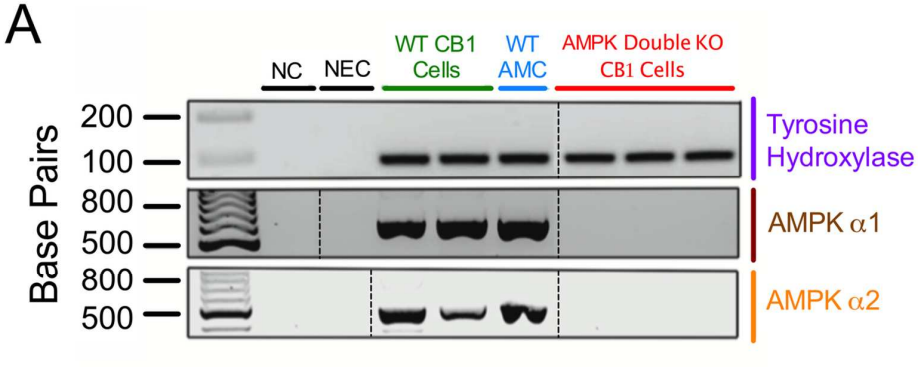

Figure 1.
61x25mm (600 x 600 DPI)

Fig. 1 cont'd

AJRCCM Articles in Press. Published on 15-December-2015 as 10.1164/rccm.201508-1667OC

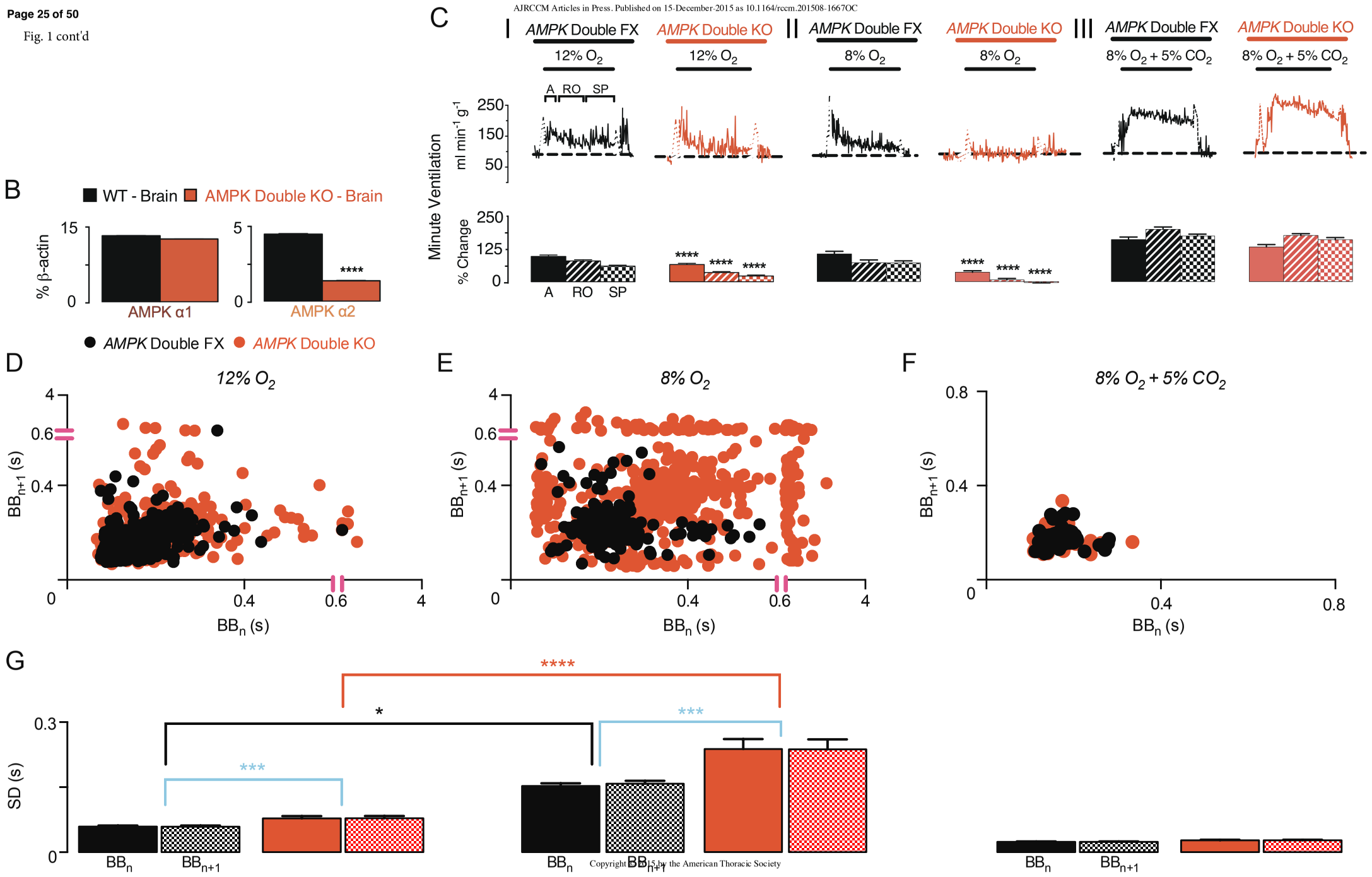

AJRCCM Articles in Press. Published on 15-December-2015 as 10.1164/rccm.201508-1667OC

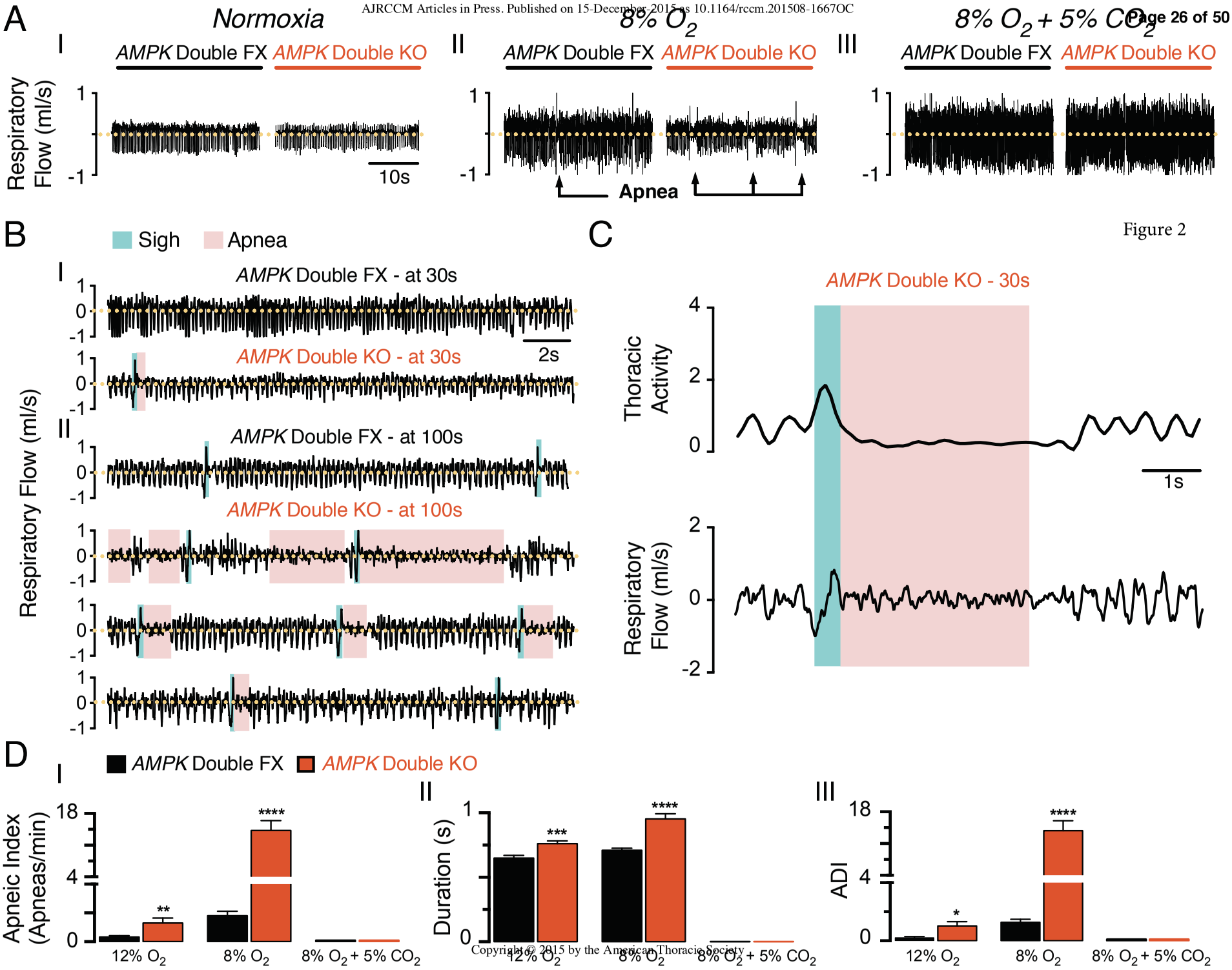

Figure 2

AJRCCM Articles in Press. Published on 15-December-2015 as 10.1164/rccm.201508-1667OC

Fig. 3

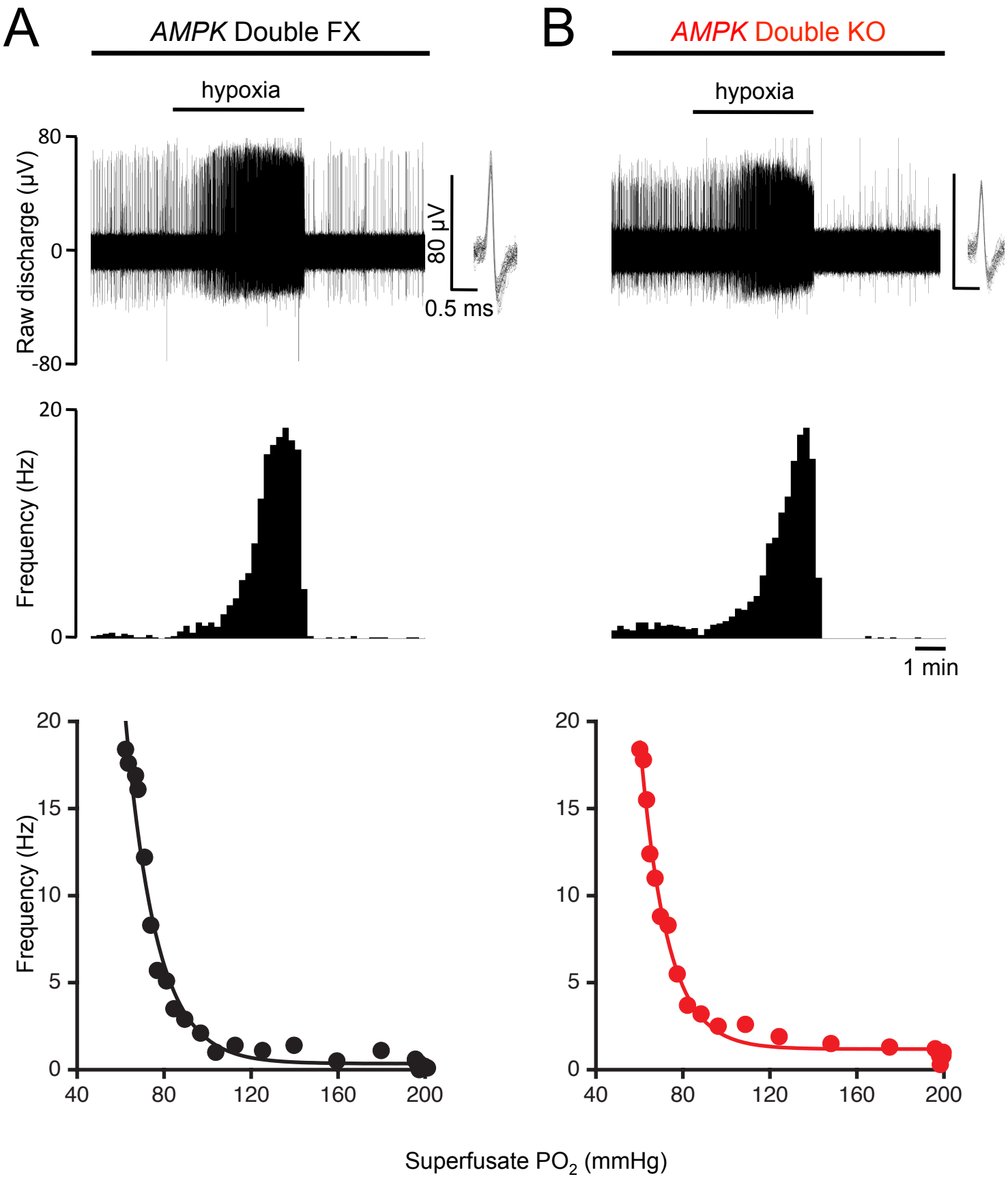

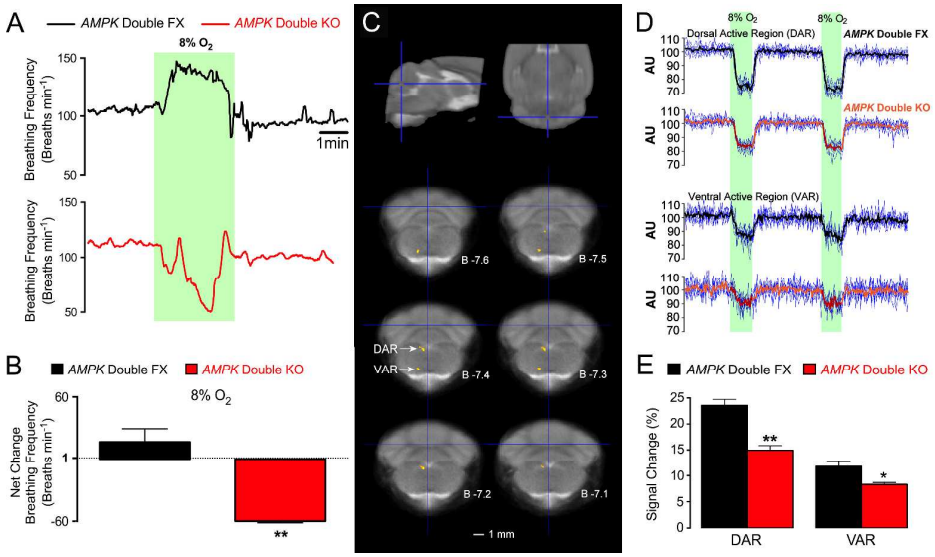

Figure 4. Functional magnetic resonance imaging demonstrates that AMPK deletion inhibits activation by hypoxia of dorsal and ventral regions of the brainstem. (A) Example records of frequency (breaths min-1) versus time during hypoxia (8% O2) for anaesthetized AMPK-α1 and -α2 double floxed (AMPK Double FX, black, n = 6) and AMPK-α1 and -α2 double knockout mice (AMPK Double KO, red, n = 6). (B) Bar charts show mean±SEM for change in breathing frequency during hypoxia; **=p< 0.01. (C) Dorsal (DAR) and ventral (VAR) active regions of brainstem that exhibited significantly lower signal change (p<0.005) during hypoxia in AMPK Double KO when compared to Double FX control mice. (D) Variability of signal time courses for DAR and VAR in blue for each individual mouse (same mice as for A, lower panel) overlaid on mean signal for AMPK Double FX (black line) and AMPK Double KO (red line); AU = arbitrary units. (E) mean±SEM percentage signal changes for DAR and VAR during hypoxia (same mice as for A, lower panel). *=p< 0.05, **=p< 0.01.
2700x1587mm (72 x 72 DPI)

AJRCCM Articles in Press. Published on 15-December-2015 as 10.1164/rccm.201508-1667OC

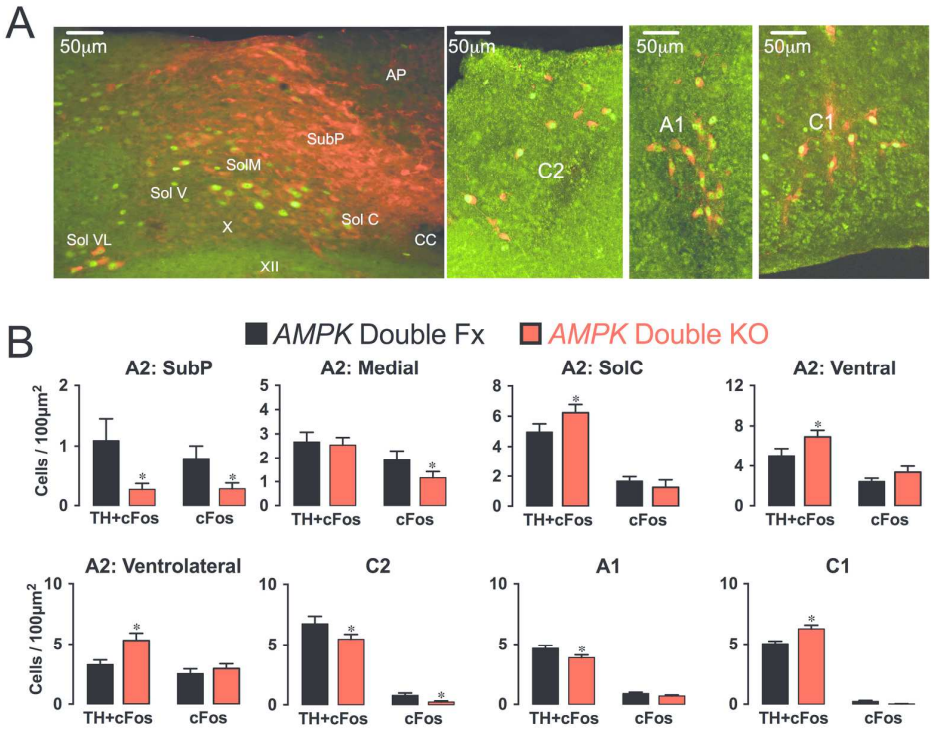

Figure 5. AMPK deletion attenuates cFOS expression in discrete areas of the NTS and ventrolateral medulla. (A) Immunostaining of a brainstem section derived from an AMPK-α1 and -α2 double knockout mouse, shows cfos (green) and Tyrosine Hydroxylase (TH, red) staining in the A2 and C2 regions of the nucleus of the solitary tract, and the ventrolateral C1/A1 region. Abbreviations: AP, area postrema; SubP, SolC, SolM, SolIM, SolDL, SolV, SolVL: Sub Postrema, commissural, medial, intermediate, dorsolateral, ventral and ventrolateral regions of the nucleus of the solitary tract; CC, central canal; IV, fourth ventricle; X, dorsal motor nucleus of the vagus; XII, hypoglossal nucleus. Scale bar 50 μm. (B) Bar charts show for each region in (A) the number of TH-positive and TH-negative cells per 1000 μm2 in which cfos expression increased during hypoxia (8%O2) for AMPK-α1 and -α2 double floxed (AMPK Double FX, black, n = 19 sections, n = 6 mice) and AMPK-α1 and -α2 double knockout mice (AMPK Double KO, red, n = 17 sections, n = 6 mice). *=p< 0.01.
168x135mm (300 x 300 DPI)

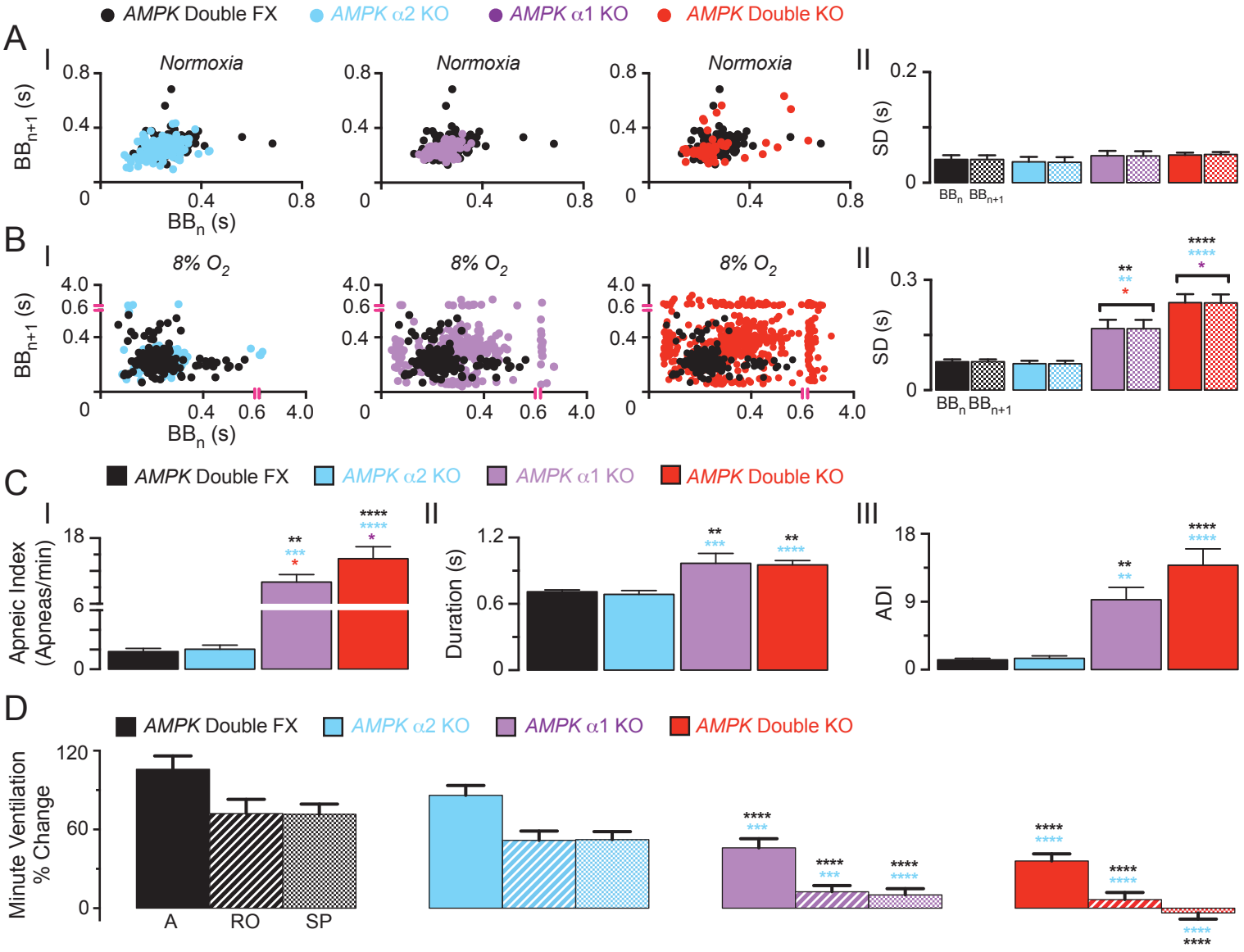

Figure 6

AJRCCM Articles in Press. Published on 15-December-2015 as 10.1164/rccm.201508-1667OC

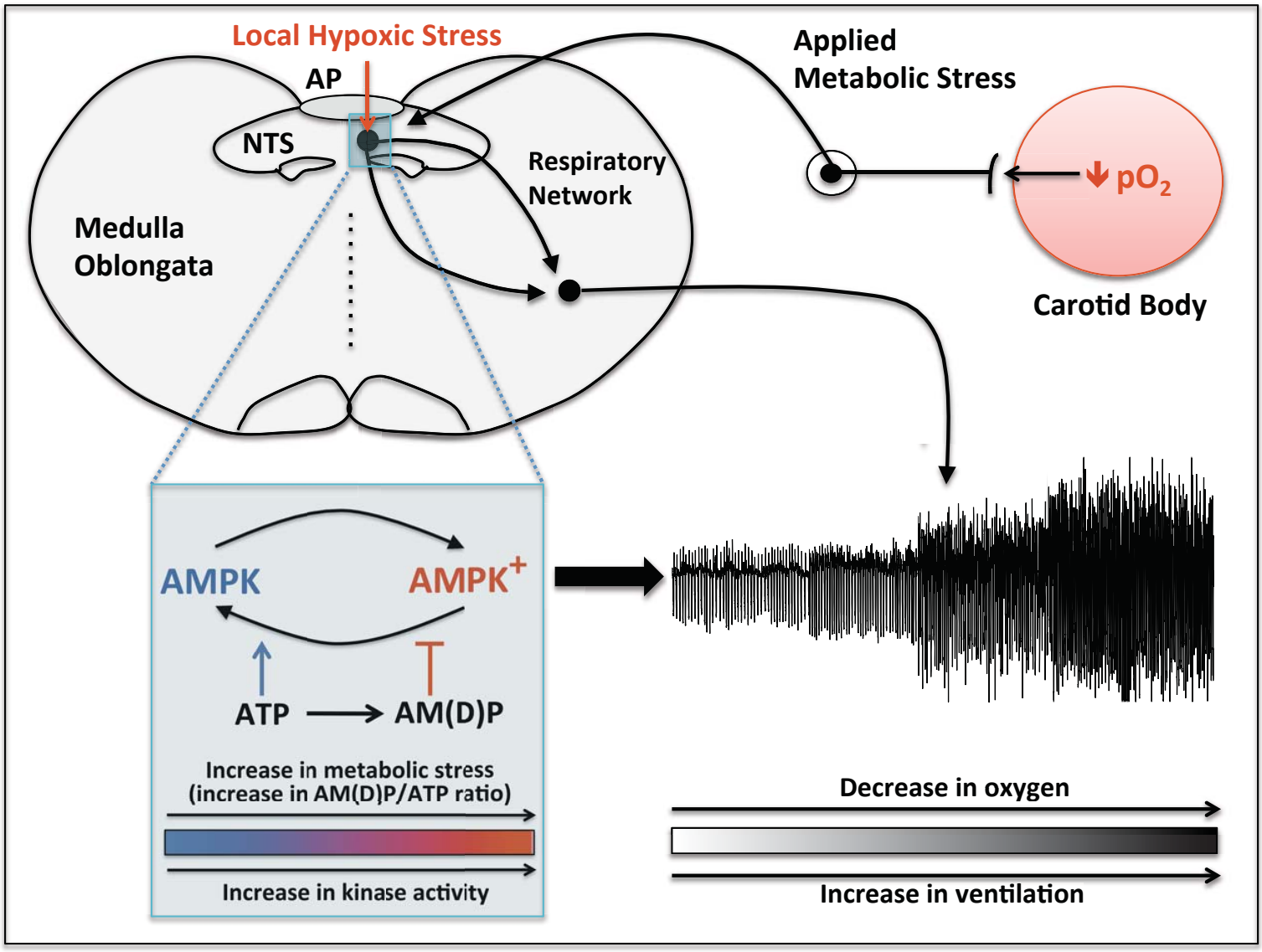

Figure 7

AJRCCM Articles in Press. Published on 15-December-2015 as 10.1164/rccm.201508-1667OC

Online Data Supplement

AMPK deficiency blocks the regulation of breathing by hypoxia and thus precipitates hypoventilation and apnea

Amira D. Mahmoud[1], Sophronia Lewis[1], Lara Juričić[2], Utibe-Abasi Udoh[1], Sandy Hartmann[1], Maurits A. Jansen[2], Oluseye A. Ogunbayo[1], Paolo Puggioni[1], Andrew P. Holmes[3], Prem Kumar[3], Jorge Navarro-Dorado[1], Marc Foretz[4,5,6], Benoit Viollet[4,5,6], Mayank B. Dutia[1], Ian Marshall[7], A. Mark Evans[1]

[1]Centre for Integrative Physiology, [2]Centre for Cardiovascular Science and [7]Centre for Clinical Brain Sciences, College of Medicine and Veterinary Medicine, University of Edinburgh, Edinburgh, UK. [3]Institute of Clinical Sciences, University of Birmingham, Birmingham, UK. [4]Institut Cochin, INSERM U1016, [5]CNRS UMR and [6]Université Paris Descartes, Paris, France.

[*]**CORRESPONDING AUTHOR**: A. Mark Evans, Centre for Integrative Physiology, College of Medicine and Veterinary Medicine, Hugh Robson Building, University of Edinburgh, Edinburgh, EH8 9XD, UK. E-mail: mark.evans@ed.ac.uk

ACKNOWLEDGMENTS

We send special thanks to Dr Cyril Pernet for advice on fMRI analysis, Dr Ian Duguid and Dr Marta Jelitai for kind help and guidance with respect to AAV injections into and imaging of the Locus Coeruleus, Dr Michael J. Shipston, Helene Widmer and Heather McClafferty for help with PCR, Dr Matthew Bailey for help and guidance with blood gas analysis, Ted Ebendal for supplying the TH-Cre mice, and Dr Renata Riha and Professor Sir Neil Douglas for helpful discussion of irregular breathing patterns and apnoeas. We also thank Steve Sawiak of the University of Cambridge for providing the mouse brain template as part of the SPMMouse project. Magnetic Resonance Imaging was carried out using the facilities of Edinburgh Preclinical Imaging, College of Medicine and Veterinary Medicine, University of Edinburgh.

AJRCCM Articles in Press. Published on 15-December-2015 as 10.1164/rccm.201508-1667OC

SUPPLEMENTARY DATA

Quantitative RT-PCR, Related to Figure 1B. AMPK-α1 expression gave (mean±SEM) Ct = 26.8 ± 0.05 (n = 3) for WT and Ct = 25.9 ± 0.02 (n = 3) for *AMPK-α1* and *-α2* double knockout mice; AMPK-α2 expression gave Ct = 28.4 ± 0.004 (n = 3) for WT and Ct = 29.1 ± 0.03 (n = 3) for *AMPK-α1* and *-α2* double knockout mice. β-actin expression gave Ct = 23.9 ± 0.03 (n = 3) for WT and Ct = 22.9 ± 0.02 (n = 3) for *AMPK-α1* and *-α2* double knockout mice

SUPPLEMENTARY METHODS

Animal studies

Experiments were performed in accordance with the regulations of the United Kingdom Animals (Scientific Procedures) Act of 1986. For statistical analysis, genotyping PCR, see Supplemental Methods. All studies and breeding were approved by the University of Edinburgh and performed under UK Home Office project licenses.

Breeding of mice and genotyping

We used conditional deletion of the genes for the *AMPK-α1* and/or *-α2* subunits, using mice in which the sequence encoding the catalytic site of either or both of the α subunits was flanked by loxP sequences (*α1flx and α2flx*; See Supplementary Reference (1)). To direct *AMPK* deletion to identified oxygen-sensing cells of the carotid body and brainstem, these were crossed with mice in which Cre recombinase was under the control of the tyrosine hydroxylase (TH) promoter. We detected the presence of wild-type or floxed *AMPK* alleles *and* CRE recombinase by PCR. 15 μl samples were run on 2% agarose gels with 10 μl SYBR®Safe DNA Gel Stain (Invitrogen) in TBE buffer against a 100 bp DNA ladder (GeneRuler^{TM}, Fermentas) using a Model 200/2.0 Power Supply (Bio-Rad). Gels were imaged using a Genius Bio Imaging System and GeneSnap software (Syngene). For tyrosine hydroxylase we used two primers: forward 5' CACCCTGACCCAAGCACT 3', reverse CTTTCCTTCCTTTATTGAGAT 3', and for Cre we used one primer: 5' GATACCTGGCCTGGTCTCG 3' (Expected size WT=290bp, Cre=430bp). We used two primers for each AMPK catalytic subunit: α1-forward: 5' TATTGCTGCCATTAGGCTAC 3', α1-reverse: 5' GACCTGACAGAATAGGATATGCCCAACCTC 3' (WT=588bp, Floxed=682bp); α2-forward 5' GCTTAGCACGTTACCCTGGATGG 3', α2-reverse: 5' GTTATCAGCCCAACTAATTACAC 3' (WT=204bp, Floxed=250bp). The PCR protocol used for all

AJRCCM Articles in Press. Published on 15-December-2015 as 10.1164/rccm.201508-1667OC

genotype primers was: 92ºC for 5min, 92ºC for 45s, 56ºC for 45sec, 72ºC for 60s, and 72ºC for 7min for 35 cycles and then 4ºC as the holding temperature.

Single-cell end-point PCR

Carotid bodies were incubated at 37°C for 25-30 min in isolation medium consisting of: 0.125mg/ml Trypsin (Sigma), 2.5mg/ml collagenase Type 1 (Worthington) made up in low Ca^{2+}/low Mg^{2+} HBSS. During this incubation the carotid bodies were separated from the associated patch of artery. The carotid bodies were then transferred to low Ca^{2+}/low Mg^{2+} HBSS containing trypsin inhibitor (0.5mg/ml) for 5min at room temperature, and then to 2ml of pre-equilibrated (95% air, 5% CO_2, 37°C) growth medium (F-12 Ham nutrient mix, 10% fetal bovine serum, 1% penicillin/streptomycin). The medium containing the carotid bodies was centrifuged and the pellet re-suspended in 100µl of growth medium. Carotid bodies were then disrupted by triturating using fire polished Pasteur pipettes.

Amplification of cDNA isolated from different individual cells was run in parallel with negative and positive controls using an initial denaturing step at 94°C for 5min and then denaturing at 94°C for 30s, annealing at 60°C for 45s, and extension for 60s at 72°C with a final 7min extension at 72°C. Initially 15 cycles were performed, followed by reaction and dilution for a further 38 cycles. To detect tyrosine hydroxylase, primers obtained from Qiagen (Quantitect Primer Assay, QT00101962) were used with an expected band length of 96bp. For the detection of AMPK two primers were used, *forward* and *reverse*, to generate an expected band length of 92bp.

Negative controls included control cell aspirants, lacking reverse transcriptase, aspiration of extracellular medium and PCR controls; these produced no detectable amplicons, ruling out genomic or other contamination. 15μl samples and a 100bp DNA ladder (GeneRuler™, Fermentas) were run on 2% agarose gels with SYBR®Safe DNA Gel Stain (Invitrogen). Gels were imaged using a Genius Bio Imaging System and GeneSnap software (Syngene). Positive controls were from samples rich in adrenomedullary chromaffin cells, dissected from adrenal glands from C57/BL6 mice. RNA was

extracted using the High Pure RNA Tissue Kit (Roche) following the manufacturer's guidelines and the concentration determined using the Nanodrop 1000 spectrophotometer (ThermoScientific). cDNA synthesis was carried out using the Transcriptor High Fidelity cDNA kit (Roche) following manufacturers instructions.

Quantitative RT-PCR

RNA from brain tissue was extracted using the High Pure RNA Tissue Kit (Roche) following the manufacturer's guidelines and the concentration determined using the Nanodrop 1000 spectrophotometer (ThermoScientific). cDNA synthesis was carried out using the Transcriptor High Fidelity cDNA synthesis Kit (Roche) following the manufacturers' instructions.

For qPCR analysis, 2.5 µl of cDNA in RNase free water was made up to 25 µl with FastStart Universal SYBR Green Master (ROX, 12.5 µl, Roche), Ultra Pure Water (8 µl, SIGMA) and fwd and rev primers for AMPK α1 and α2. The sample was then centrifuged and 25 µl added to a MicroAmp^{TM} Fast Optical 96-Well Reaction Plate (Greiner bio-one), the reaction plate sealed with an optical adhesive cover (Applied Biosystems) and the plate centrifuged. The reaction was then run on a sequence detection system (Applied Biosystems) using AmpliTaq Fast DNA Polymerase, with a 2min initial step at 50^{o}C, followed by a 10min step at 95^{o}C, then a 15s step at 95^{o}C which was repeated 40 times. Then a dissociation stage with a 15s step at 95^{o}C followed by a 20s at 60^{o}C and a 15s step at 95^{o}C. Negative controls included control cell aspirants for which no reverse transcriptase was added, and aspiration of extracellular medium and PCR controls. None of the controls produced any detectable amplicon, ruling out genomic or other contamination.

Viral injections of double-floxed reporter gene

We made lateral injections adjacent to one of two readily identifiable clusters of catecholaminergic neurons, namely the locus coeruleus and nigrostriatal region. Injections proximal to the locus coeruleus

AJRCCM Articles in Press. Published on 15-December-2015 as 10.1164/rccm.201508-1667OC

[anteroposterior (AP), 4.122 mm; mediolateral (ML), +/– 1.28 mm; dorsoventral (DV) 3.65 mm] were made through an internal cannula at a rate of 100 nl/min for 2.5 min (250nl total volume). After surgical procedures, animals were allowed to recover for at least one week. The mice were then perfused and brain extracted and sagittally sectioned (60μm thick) using a vibratome. For co-localization experiments, brain sections from eYFP-transduced mice were incubated in mouse anti-tyrosine hydroxylase (1:1000, Millipore, MAB-318). Sections were then incubated in goat anti-rabbit IgG secondary antibody (1:750, Invitogen, A594).

Measurement of arterial oxygen saturation heart rate and blood pressure

Arterial $sp\mathrm{O_2}$ measurements and heart rate of mice were made by infrared using the MouseSTAT™ Pulse Oximeter (Kent Scientific, USA) and paw sensor (anesthetized) or Y-style tail sensor (conscious), with blood pressure recorded using a CODA STANDARD non-invasive blood pressure system (Kent Scientific, USA).

Venous blood gas analysis

Gas analysis (ABL90 Radiometer, Copenhagen) was performed on blood collected from the vena cava under terminal anaesthesia (Thiobutabarbital sodium, 120mg/kg IP). Blood was drawn into a heparin-coated syringe and analysis was performed within 1 minute of collection.

Isolated carotid body

Single fibre chemoafferent activity was amplified and filtered and recorded using a 1401 interface running Spike 2 software (Cambridge Electronic Design). Single- or few-fibre chemoafferent recordings were made from carotid bifurcations held in a small volume tissue bath, and superfused (36-37°C) with gassed (95% O_2 and 5% CO_2), bicarbonate-buffered saline solution (composition (mM): 125 NaCl, 3 KCl, 1.25 NaH_2PO_4, 5 Na_2SO_4, 1.3 $MgSO_4$, 24 $NaHCO_3$, 2.4 $CaCl_2$). Hypoxic gas tensions were

maintained and calibrated via a blood gas analyser.

Plethysmography

We used a Halcyon low noise pneumatochograph and FinePointe acquisition and analysis software (Buxco Research Systems, UK). Following 10-20 min of acclimation under normoxia mice were exposed to hypoxia (8% O_2, with 0.05% CO_2, balanced with N_2), or hypoxia+hypercapnia (8% O_2, 5% CO_2, balanced with N_2). Throughout our analyses, we defined an apnea as a period of cessation of breathing that was greater than the average duration, including interval, of 2 successive breaths (~600 ms) of control mice during normoxia. For these analyses we also utilized a threshold below which any event was considered to be within the signal noise (0.25 mmHg = standard deviation of noise).

Computational analysis of thoracic movements

Movements were captured using a digital camera synchronized with data acquisition via plethysmography. Within each frame of the movie we defined a region-of-interest (ROI) covering the side of the thorax of the mouse, low-pass filtered the MI at 10 Hz and calculated the motion index (MI) for each successive frame as:

$$\mathrm{MI}_f = \Sigma_{i=1}^{N} (c_{f+1,i} - c_{f,i})^2$$

where $c_{f,i}$ is the grayscale level of the pixel i of the ROI in the frame f.

Functional magnetic resonance imaging

Six *AMPK-α1flx and -α2flx* and six *AMPK-α1* and *-α2* double knockout mice were imaged on a 7-T horizontal bore MRI scanner (Agilent Technologies, Yarnton, UK), equipped with a high-performance gradient insert (12-cm inner diameter, maximum gradient strength 400 mT/m). The mice were anesthetized with 0.8-1.3% isoflurane in air, placed in a cradle (Rapid Biomedical GmbH, Rimpar,

AJRCCM Articles in Press. Published on 15-December-2015 as 10.1164/rccm.201508-1667OC

Germany), and the skull was fixed with plastic ear bars. Rectal temperature was monitored throughout the experiments, and body temperature was maintained at 37°C with a hot air fan. Respiration rate was monitored using a pressure pad sensor placed under the animal. A birdcage coil (72-mm diameter) was used for radio frequency transmission and a mouse 2-channel phased array brain coil for signal reception. All sequences were acquired with the following parameters: field-of-view 19.2 mm×19.2 mm, 30 contiguous coronal slices of 0.4 mm thickness. Whole brain structural images were acquired using a fast spin echo sequence (echo train length 8) with the following parameters: repetition time (TR) = 3,100ms, effective echo time = 36 ms; 8 signal averages, acquisition matrix 192 x 192, zero-filled to 256x256.

After this scan, functional image acquisition was started during which the concentration of the inhaled oxygen was altered: 5min normoxia (21% O_2) was followed by two 2min periods of hypoxia (8% O_2), with 7min of normoxia after each hypoxic period. Two hundred and thirty fMRI volumes were collected using a 3-shot Echo Planar Imaging sequence with the following parameters: effective repetition time (TR) = 6,000 ms (2,000ms per shot), effective echo time = 7.08 ms; flip angle 90°, 1 signal average, acquisition matrix 64 x 64.

SPM8 (Wellcome Trust Centre for Neuroimaging, University College London, UK) was used for image analysis. Whole brain structural images were acquired using a fast spin echo sequence (echo train length 8) with the following parameters: repetition time (TR) = 3,100ms, effective echo time = 36 ms; 8 signal averages, acquisition matrix 192 x 192, zero-filled to 256x256. Bias corrected (www.slicer.org) structural images were coregistered to a template (www.spmmouse.org) and averaged to create a study-specific structural template. Functional data of each animal was realigned to the mean volume in the series, and then spatially normalized according to SPM8 co-registration procedures using each individual animal's structural scan, and smoothed with a 0.7x0.7x4 mm full width half maximum (FWHM) Gaussian filter.

First level statistical analysis (Figure E7) was performed using a general linear model implemented in

SPM8. The design matrix of the linear model incorporated a zero polynomial, estimated brain motion parameters, respiration rate signal and a predicted BOLD response which is obtained by convolving the boxcar of the block design with the SPM8 canonical hemodynamic response function. For each animal, a statistical parametric map of the *t*-statistic was generated for the (normoxia < hypoxia) signal contrast. Second-level (group) analysis and between-group differences were investigated using a two-sample t-test in SPM8. The second level t-map for the contrast (knockout > control) was thresholded at a level of $P<0.005$ with a cluster threshold of 4 voxels (SPM8). A region of interest tool (http://marsbar.sourceforge.net/) was used to analyze the nature of between-group differences. For regions which showed significant group differences, the mean signal time series for each animal was computed by averaging all the voxel signals within each region at each time point. Finally, the percentage signal changes were calculated for each region and the group means compared.

TH labeling and cFOS Expression

Mice were deeply anesthetized and transcardially perfused 90 minutes after a single exposure to hypoxia (8% O_2) and the 44 μM sections of the brainstem were cut by microtome. Alternate sections were collected together and processed by free-floating immunocytochemistry to detect FOS immunoreactivity and stain for TH positive cells. For cell counting see supplemental procedures.

Brain sections were incubated overnight with shaking at 4^{o}C in anti-FOS (polyclonal raised in rabbit, used at 1:10000, Calbiochem) and anti-tyrosine hydroxylase (raised in mouse; 1:1000, Millipore) antibodies diluted in blocking buffer. Sections were then incubated in biotinylated secondary anti-rabbit antibody raised in goat, 1:500 (Vector Labs) which served to amplify the FOS staining. This was followed by incubation with secondary fluorescent conjugated antibodies (Alexa Fluor® 488-streptavidin and Alexa Fluor ®568, 1:500 dilutions, Molecular Probes, Inc).

AJRCCM Articles in Press. Published on 15-December-2015 as 10.1164/rccm.201508-1667OC

Two investigators independently quantified the number of FOS and TH positive cells in brainstem sections, blinded to the treatments at the time of counting. Images of the regions were acquired using a Leica digital camera, controlled by Leica acquisition software (AIS), and attached to an upright Leica microscope and x10 objective. Using ImageJ, these images were converted to 8 bit, thresholded using the same parameters, and TH- and FOS-positive cells counted using the Analyze Particles macro. The conditions for thresholding and for the macro were determined in part by comparing count results with manually counted images and ensuring that counts made manually and via the software matched for 20 regions. Non-overlapping, multiple regions of interest (ROI) were used. The number of FOS-positive cells within each ROI were normalized by the surface area of that ROI to allow comparison.

SUPPLEMENTARY REFERENCES

1. Lantier L, Fentz J, Mounier R, Leclerc J, Treebak JT, Pehmoller C, Sanz N, Sakakibara I, Saint-Amand E, Rimbaud S, Maire P, Marette A, Ventura-Clapier R, Ferry A, Wojtaszewski JF, Foretz M, Viollet B. AMPK controls exercise endurance, mitochondrial oxidative capacity, and skeletal muscle integrity. *FASEB J.* 2014; 28: 3211-3224.

SUPPLEMENTARY FIGURES

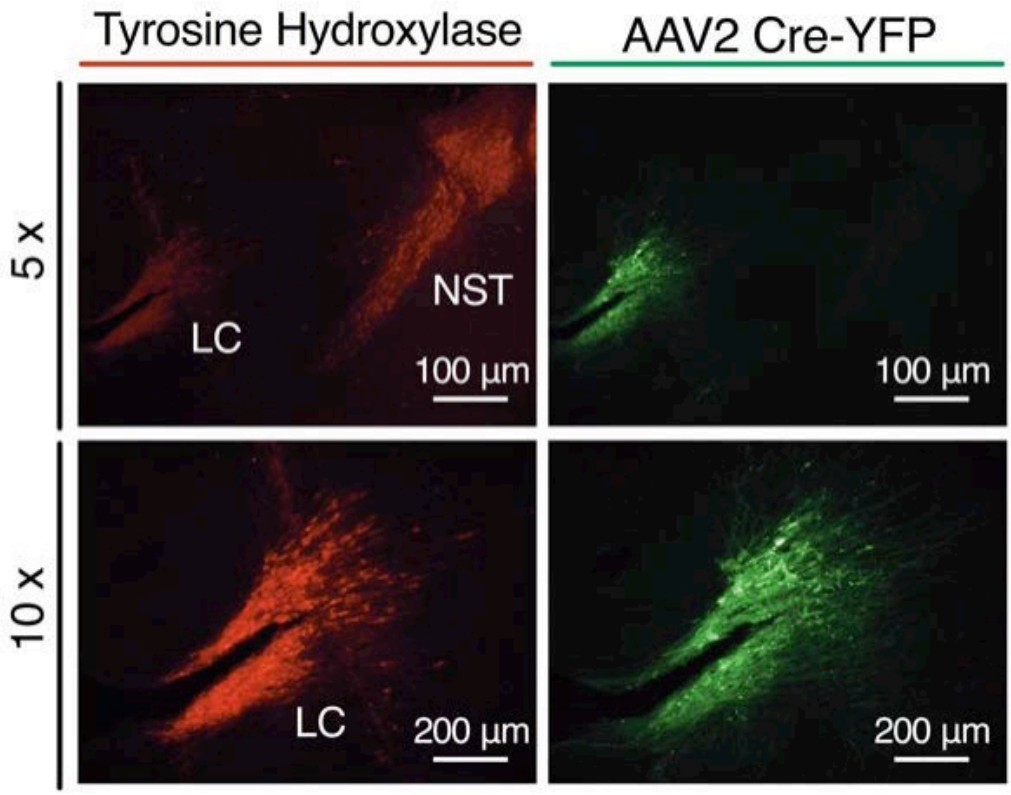

Figure E1. Cre expression in tyrosine hydroxylase expressing cells. Images of sagittal sections from the brain of a TH-Cre mouse after injection of AAV1/2 Cre-induced YFP virus into the locus coeruleus (LC) but not the nigrostriatal region (NST), *left panels* show immunostaining depicting tyrosine hydroxylase immunoreactivity (red) and *right panels* show Cre-induced YFP expression (green). *Upper panels* show 5x magnification, *lower panels* show 10x magnification.

AJRCCM Articles in Press. Published on 15-December-2015 as 10.1164/rccm.201508-1667OC

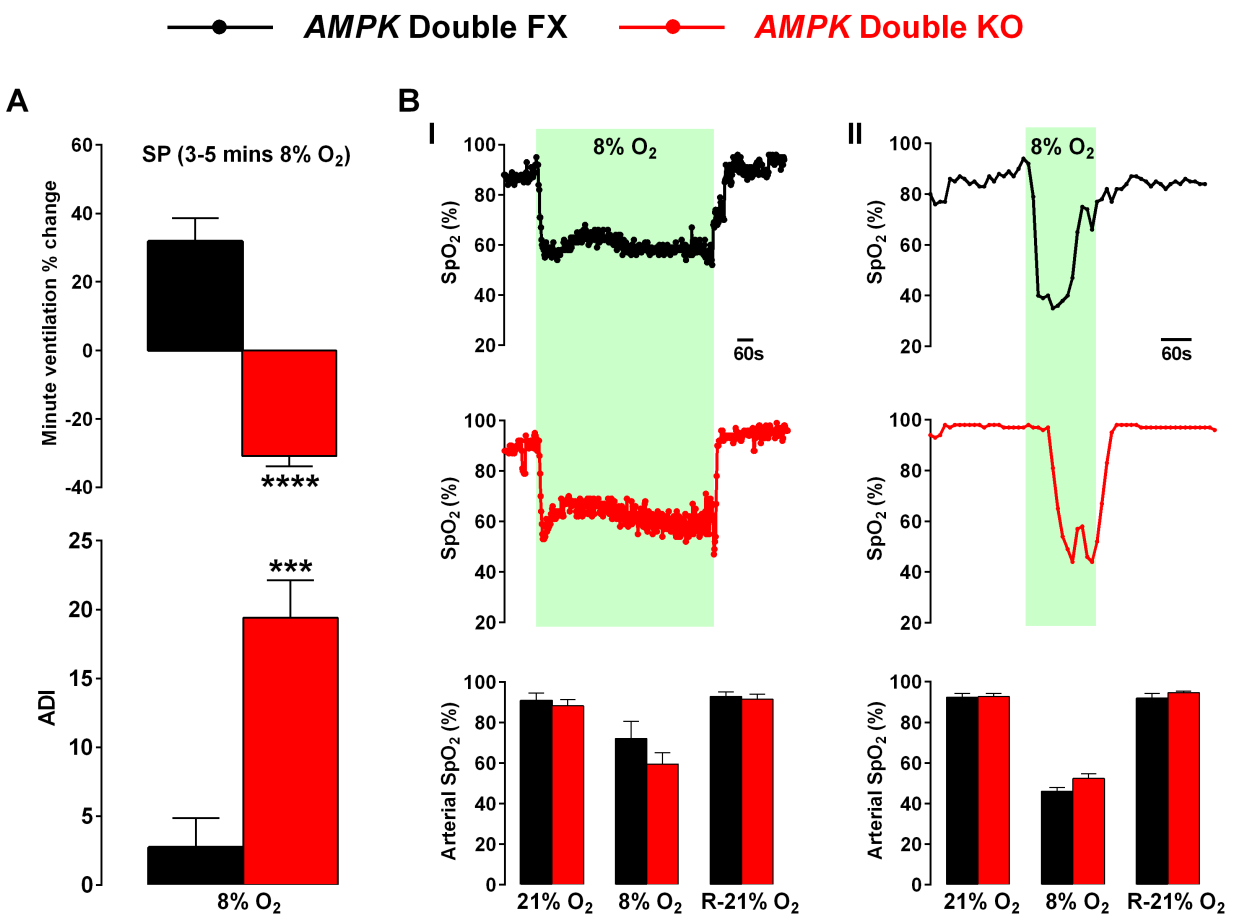

Figure E2. Conditional deletion of *AMPK* catalytic α-subunits in tyrosine hydroxylase expressing cells markedly attenuates the hypoxic ventilatory response at similar levels of arterial O_2 saturation. (*A*) Bar charts show mean±SEM for the minute ventilation (ml min^{-1} g^{-1}; *upper panel*) of *AMPK-α1* and *-α2* floxed (*AMPK* Double FX, n=3) and *AMPK- α1* and *-α2* double knockout (*AMPK* Double KO, n=3) during the plateau (3-5min) of the Sustained Phase (SP) of the hypoxic ventilatory response. *Lower panel* shows mean±SEM for the apnoea-duration index (frequency x duration; n=3); *** = $p < 0.001$, **** = $p < 0.0001$. (*B*) Exemplar records from conscious (I) and anesthetized (II) *AMPK* Double FX (upper panel, black, n=3) and *AMPK* Double KO mice (middle panel, red, n=3) show the time course of changes in arterial oxygen saturation (spO_2). *Lower panels* show bar charts of mean±SEM for arterial spO_2 during normoxia, hypoxia (8% O_2) and recovery during normoxia.

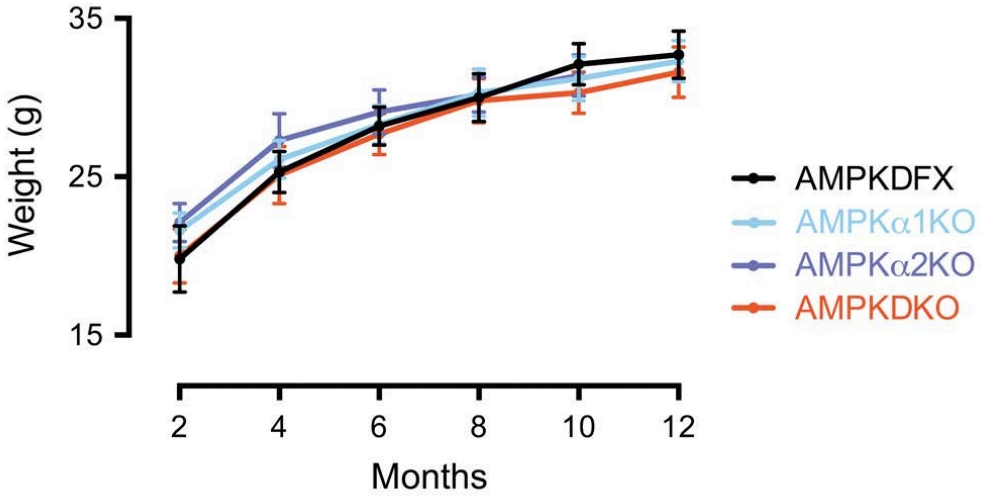

Figure E3. Body weight versus age of control and knockout mice. Values shown are mean±s.e.m. for body weight (g) versus age from 2 months to 12 months in 2 month intervals in the *AMPK-α1* and *-α2* double floxed (*AMPK* Double FX), *AMPK-α1* knockout (*AMPK-α1* KO), *AMPK-α2* knockout (*AMPK-α2* KO) and *AMPK-α1* and *-α2* double knockout (*AMPK* DKO) mice.

AJRCCM Articles in Press. Published on 15-December-2015 as 10.1164/rccm.201508-1667OC

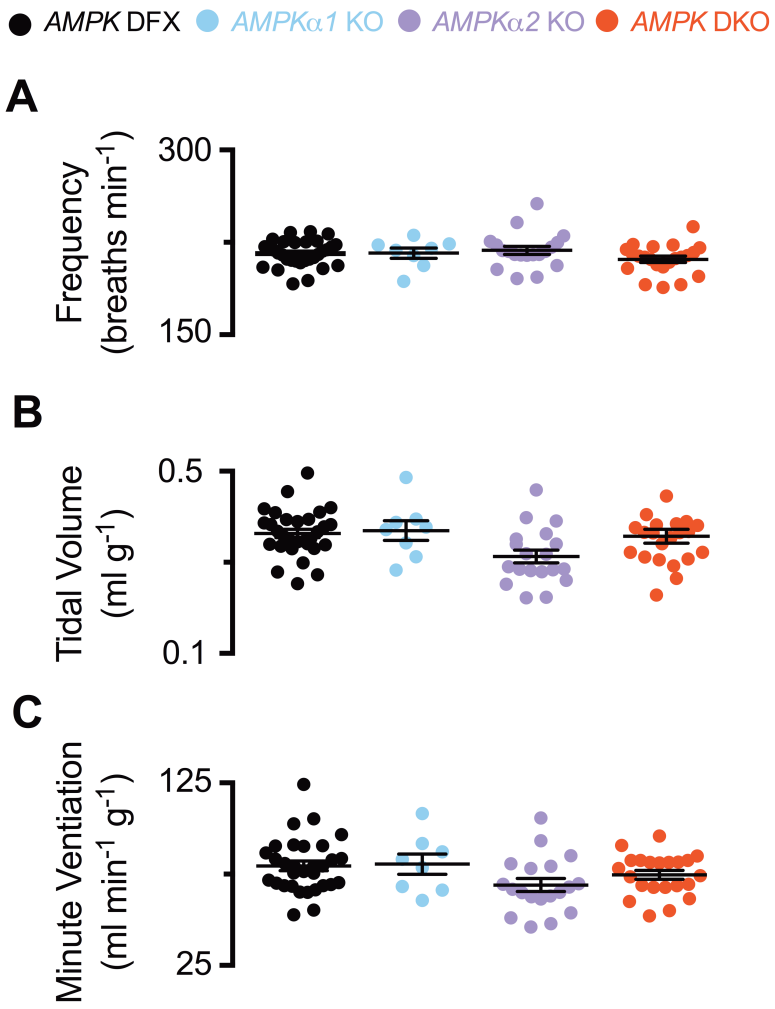

Figure E4. Breathing frequency, tidal volume and minute ventilation of experimental mice during normoxia. Scatter plots show individual points and mean±SEM for breathing frequency (min^{-1}, *upper panel*) tidal volume (ml g^{-1}, *middle panel*) and minute ventilation (ml min^{-1} g^{-1}, *lower panel*) under normoxia for *AMPK-α1* and *-α2* double floxed (black, n = 31), *AMPK-α1* knockout (*AMPK-α*1 KO, blue, n=19), *AMPK-α2* knockout (*AMPK-α2* KO, mauve, n=16), *AMPK-α1* and *-α2* double knockout mice (*AMPK* DKO, red, n = 22).

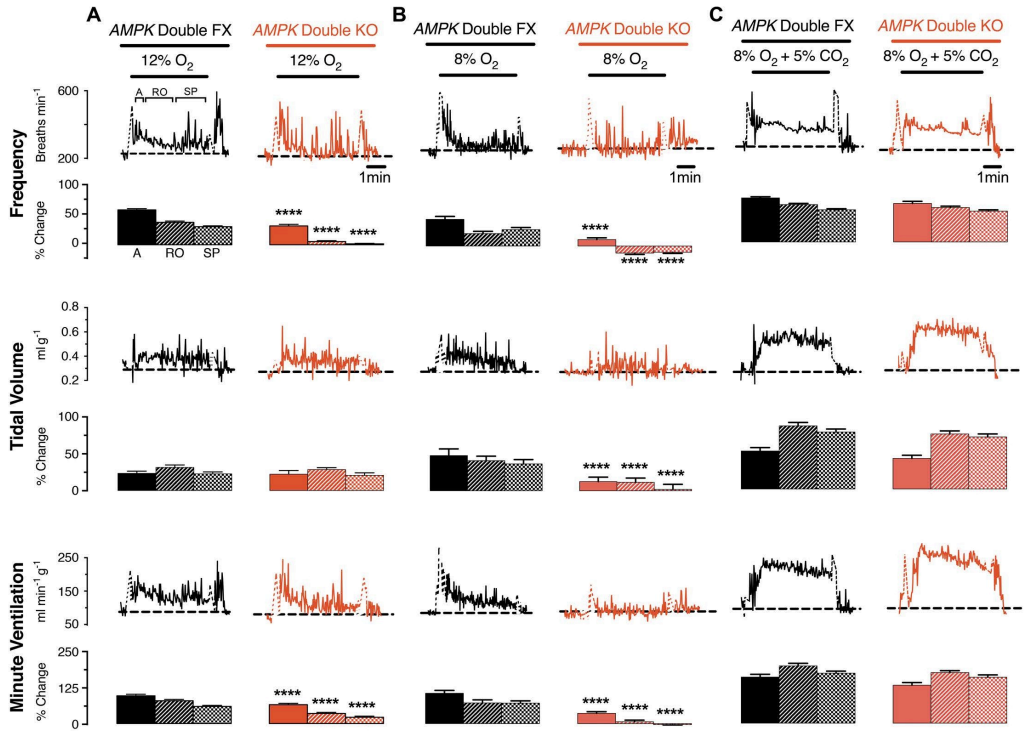

Figure E5. Effect of AMPK deletion on breathing frequency, tidal volume and minute ventilation during hypoxia. *Upper panels* show example records of minute ventilation (ml min^{-1} g^{-1}) versus time during 12% O_2 (D) 8% O_2 and (E) 8% O_2 with 5% CO_2 for *AMPK-α1* and *-α2* double floxed (*AMPK* Double FX, black, n = 31) and *AMPK-α1* and *-α2* double knockout mice (*AMPK* Double KO, red, n = 22). *Lower panels*, Bar charts show mean±s.e.m. for increase in minute ventilation for the peak of the Augmenting Phase (A), after 100s of Roll Off (RO) and the plateau of the Sustained Phase (SP) of the response to hypoxia; ****=p< 0.0001.

AJRCCM Articles in Press. Published on 15-December-2015 as 10.1164/rccm.201508-1667OC

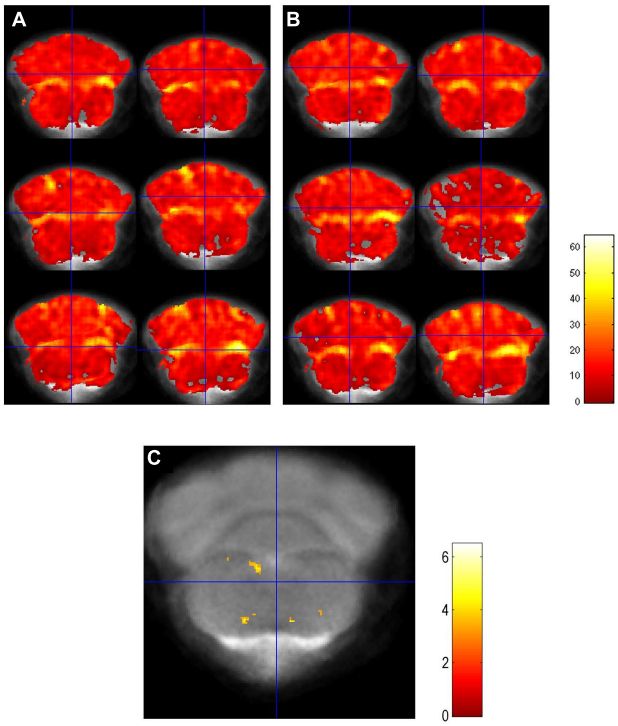

Figure E6. First and second level fMRI analysis. First level statistical analysis, changes in BOLD signal level during hypoxia (versus normoxia) were mapped for each animal; note, almost the entire brain shows highly significant signal reduction for both: **(***A***)** the six Double-KO; **(***B***)** the six Double-FX mice; (*C*) Second level of analysis, a two-sample t-test was performed to compare the BOLD responses of Double-KO and Double-FX during hypoxia. We thus identified brainstem regions demonstrating a reduced response in the Double-KO group versus the Double-FX group, which are overlaid on the study-specific brain template with a statistical threshold of $p<0.005$ ($t = 3.2$). Colour scale indicates t-score.

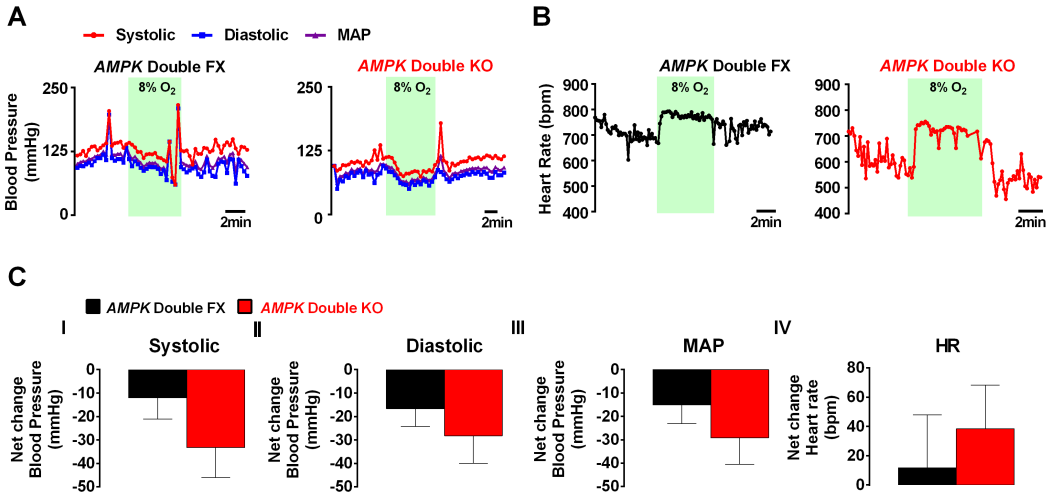

Figure E7. Blood pressure and heart rate during normoxia and hypoxia. Data show for control and *AMPK-α1* and *-α2* double knockout (*AMPK* Double KO) mice: (*A*) Time course for changes in blood pressure during hypoxia (8% O_2). (*B*) Time course for changes in heart rate during hypoxia (8% O_2). (*C*) Mean±s.e.m. for systolic blood pressure, diastolic blood pressure, mean arterial blood pressure (MAP) and heart rat (HR) during normoxia, hypoxia and recovery. (n=3).

AJRCCM Articles in Press. Published on 15-December-2015 as 10.1164/rccm.201508-1667OC

Table E1. Blood gases and pH

	AMPK Double Floxed	*AMPK* α1 Knockout	*AMPK* α2 Knockout	*AMPK* Double Knockout	Significance
pO_2 (mmHg)	52.5 ± 2.5	53.8 ± 9.4	47.0 ± 6.8	57.3 ± 8.9	ns
	n = 5	n = 4	n = 4	n = 4	
pCO_2 (mmHg)	52.5 ± 5.5	54.3 ± 10.0	57.5 ± 2.1	64.8 ± 6.7	ns
	n = 5	n = 4	n = 4	n = 4	
pH	7.2 ± 0.02	7.2 ± 0.09	7.2 ± 0.01	7.1 ± 0.02	ns
	n = 5	n = 4	n = 4	n = 7	

SUPPLEMENTARY MOVIES

Movie E1. Exposure of an *AMPK-α1* and *-α2* double floxed (*AMPK Double FLX*) mouse to hypoxia (8% O_2).

Movie E2. Exposure of an *AMPK-α1* and *-α2* double knockout (*AMPK* Double KO) mouse to hypoxia (8% O_2).